

Bayesian Function-on-Function Regression for Spatial Functional Data

Heesang Lee¹, Dagon Oh¹, Sunhwa Choi³, and Jaewoo Park^{1,2}

¹Department of Statistics and Data Science, Yonsei University

²Department of Applied Statistics, Yonsei University

³Innovation Center for Industrial Mathematics, National Institute for
Mathematical Sciences

August 23, 2024

Abstract

Spatial functional data arise in many settings, such as particulate matter curves observed at monitoring stations and age population curves at each areal unit. Most existing functional regression models have limited applicability because they do not consider spatial correlations. Although functional kriging methods can predict the curves at unobserved spatial locations, they are based on variogram fittings rather than constructing hierarchical statistical models. In this manuscript, we propose a Bayesian framework for spatial function-on-function regression that can carry out parameter estimations and predictions. However, the proposed model has computational and inferential challenges because the model needs to account for within and between-curve dependencies. Furthermore, high-dimensional and spatially correlated parameters can lead to the slow mixing of Markov chain Monte Carlo algorithms. To address these issues, we first utilize a basis transformation approach to simplify the covariance and apply projection methods for dimension reduction. We also develop a simultaneous band score for the proposed model to detect the significant region in the regression function. We apply our method to both areal and point-level spatial func-

tional data, showing the proposed method is computationally efficient and provides accurate estimations and predictions.

Keywords: dimension reduction; function-on-function regression; functional kriging; Markov chain Monte Carlo; Gaussian process

1 Introduction

With the improvement in data collection technology, data have become large, complex, and high-dimensional. To analyze such datasets, functional data analysis has been developed in many disciplines, including linear models, nonparametric methods, and multivariate techniques (cf. Ramsay and Silverman, 2005). Although most functional data analysis methods assume independence between functions, there is an increasing interest in modeling dependent functions. An important example is spatial functional data (Delicado et al., 2010; Martínez-Hernández and Genton, 2020), where we observe a curve with a spatial component. In this manuscript, we propose a Bayesian approach for spatial functional regression, allowing both the predictor and response as functional variables. The proposed method can carry out functional kriging and study the relationships between functional variables. For efficient computation, we utilize basis transformation approaches (Zhang et al., 2016; Kowal and Bourgeois, 2020) and projection methods (Hughes and Haran, 2013; Park and Lee, 2022; Lee and Haran, 2022).

There is a vast literature on modeling functional variables in the regression context. Just a few of these include scalar-on-function regression models (Cardot et al., 1999; Reiss et al., 2017), function-on-scalar regression models (Ramsay and Silverman, 2005; Reiss et al., 2010), and function-on-function regression models (Ivanescu et al., 2015; Kim et al., 2018). These models extend the standard regression by taking responses or covariates (or both) as functional variables. However, most previous studies assume independent random errors, which is unsuitable for spatial functional data.

There have been several works to account for spatial correlations in the model. Zhang et al. (2016) developed a function-on-scalar regression based on conditional autoregressive models. For scalar-on-function regression, Pineda-Ríos et al. (2019) proposed a functional simultaneous autoregressive model to study econometric data. Recently, Kang et al. (2023) proposed a sparse

functional spatial generalized linear mixed model in a Bayesian framework that is computationally efficient. Note that the prediction of curves at unobserved locations is one of the main interests in many geostatistical problems. The previous works focused on estimating functional parameters, not functional prediction (i.e., functional kriging). Furthermore, function-on-function regression models for spatially correlated data have not been studied.

In terms of functional kriging, Goulard and Voltz (1993) proposed the exploratory method based on the stationarity assumption. They reconstructed the complete curves via a parametric model by assuming that the curves were only known at a finite set of points. By extending this, Giraldo et al. (2011) proposed nonparametric approaches based on the B-splines basis representation. Caballero et al. (2013) developed a functional universal kriging (UK) that allows a different mean trend of functions. Menafoglio et al. (2013) established a theoretical framework for UK under a general Hilbert space. All of these approaches focused on curve prediction based on variogram fittings; therefore, it is challenging to study the relationships between functional variables. Furthermore, it is not trivial to quantify uncertainties for functional parameters.

In this manuscript, we develop a spatial function-on-function regression (SFoFR), extending the standard FoFR by including spatial random functions. For Bayesian inference, we utilize a basis transformation approach (Zhang et al., 2016; Kowal and Bourgeois, 2020) that can convert every observed function from the data space into the basis space. From this, we can fit the model with a simpler covariance in the basis space while still allowing a flexible form of it in the data space. However, Bayesian inference for SFoFR is still challenging, even with a moderate sample size. With an increasing sample size, the number of spatially correlated parameters grows, resulting in the slow mixing of the Markov chain Monte Carlo (MCMC) algorithm. Therefore, we adopt projection methods (Hughes and Haran, 2013; Lee and Haran, 2022) to reduce the dimension of spatially correlated parameters. The projection-based SFoFR (PSFoFR) is computationally efficient and provides accurate estimations and predictions. Our framework is applicable to both discrete and continuous domains, covering the broader class of spatial functional data.

The remainder of this manuscript is organized as follows. In Section 2, we explain the background of the existing methods. In Section 3, we propose a PSFoFR and describe functional kriging. Furthermore, we provide theoretical justification for our method. In Section 4, we provide simulation studies to investigate the performance of the proposed methods. In Section

5, we apply the method to real datasets, including Japan PM2.5 data and Korea mobility data. We conclude with a summary and discussion in Section 6.

2 Background

2.1 Spatial Functional Regression

Functional regression models have been studied for both areal and point-level data. For areal data, Zhang et al. (2016) developed function-on-scalar regressions with nonseparable and non-stationary covariance structures. They used a basis transformation approach to make inference scalable to higher dimensional problems. Kang et al. (2023) proposed scalar-on-function regression based on sparse representation of high-dimensional spatial random effects. Both of these approaches modeled spatial correlations through Gaussian Markov random fields. For point-level data, Aristizabal et al. (2019) proposed the analysis of variance of spatial functional data, and Římalová et al. (2022) developed a permutation testing approach. Both methods are based on variogram fittings from the residuals of independent function-on-scalar regression models. Park et al. (2023) developed a scalar-on-function regression model with a low-rank representation of spatially dependent functional covariates.

Although functional kriging is one of the important geostatistical goals, most previous approaches focused on parameter estimation. Furthermore, existing methods take either responses or covariates as functional variables, but not both. Therefore, it is challenging to study the relationships between functional variables in the presence of spatial correlations. In Section 3, we propose a Bayesian framework for SFoFR that can be applicable to both areal and point-level data. The Bayesian approach is convenient for complex hierarchical models because we can carry out estimation and prediction using posterior samples.

2.2 Spatial Functional Kriging

As a seminal work, Goulard and Voltz (1993) considered both multivariate and functional kriging approaches to predict function values. In terms of multivariate perspectives, they regarded the vector of observed values from each curve as a multivariate random variable. Then, they used

cokriging to predict the values of the multivariate random vector. As a functional approach, Goulard and Voltz (1993) defined the best linear unbiased predictor (BLUP) of curves at unobserved sites and fitted each curve with a parametric model. Extending such approaches, Giraldo et al. (2011) proposed functional ordinary kriging (OK) by replacing parametric models with nonparametric models based on cubic B-splines. Then, they constructed BLUP of the OK predictor. However, they still assume stationarity among functions, which has limited applicability. To address this, universal kriging (UK) approaches that allow different mean functions have been developed (Caballero et al., 2013; Menafoglio et al., 2013). Here, we describe the UK following Caballero et al. (2013), and the results can be extended to general Hilbert spaces (Menafoglio et al., 2013).

Consider we have a non-stationary stochastic process $\{Y_{\mathbf{s}}(t), t \in \mathcal{T}, \mathbf{s} \in \mathcal{D}\}$ in $\mathcal{L}^2(\mathcal{T})$, the set of all square integrable functions on $\mathcal{T} \in \mathbb{R}$ defined over the spatial domain $\mathcal{D} \in \mathbb{R}^2$. Then, the i th observed curve realized from the random process can be modeled as

$$Y_{\mathbf{s}_i}(t) = \mathbf{X}'_{\mathbf{s}_i} \boldsymbol{\beta}(t) + v_{\mathbf{s}_i}(t), \quad (1)$$

where $\mathbf{X}'_{\mathbf{s}_i} \in \mathbb{R}^L$ is a vector of spatial variables at location \mathbf{s}_i and $\boldsymbol{\beta}(t) = (\beta_1(t), \dots, \beta_L(t))'$ is the corresponding regression function vector. In addition, $v_{\mathbf{s}_i}(t)$ is a functional error term from a zero-mean second-order stationary and isotropic random process $\{v_{\mathbf{s}}(t), t \in \mathcal{T}, \mathbf{s} \in \mathcal{D}\}$ in $\mathcal{L}^2(\mathcal{T})$. Note that (1) allows the non-constant spatial mean function (drift) and belongs to a function-on-scalar regression framework.

The UK approaches can select an optimal linear model for a given n number of observations $Y_{\mathbf{s}_1}(t), \dots, Y_{\mathbf{s}_n}(t)$. Furthermore, UK approaches can predict $Y_{\mathbf{s}_1^*}(t)$ for an unobserved location \mathbf{s}_1^* by accounting for the spatial dependence structure in the model. The BLUP of the UK predictor at \mathbf{s}_1^* is

$$\hat{Y}_{\mathbf{s}_1^*}(t) = \sum_{i=1}^n \lambda_i Y_{\mathbf{s}_i}(t), \quad (2)$$

where the weight $\boldsymbol{\lambda} = (\lambda_1, \dots, \lambda_n)'$ is obtained by minimizing the global variance of the prediction error under the following unbiasedness constraint:

$$\min_{\lambda_1, \dots, \lambda_n} \text{Var}(\hat{Y}_{\mathbf{s}_1^*}(t) - Y_{\mathbf{s}_1^*}(t)), \quad \text{s.t.} \quad \mathbb{E}[\hat{Y}_{\mathbf{s}_1^*}(t) - Y_{\mathbf{s}_1^*}(t)] = 0. \quad (3)$$

Caballero et al. (2013); Menafoglio et al. (2013) showed that the optimal weight $\boldsymbol{\lambda}$ in (3), can be obtained by solving the following linear equation.

$$\begin{pmatrix} C_{11} & \cdots & C_{1n} & \mathbf{X}'_{\mathbf{s}_1} \\ \vdots & \ddots & \dots & \vdots \\ C_{n1} & \cdots & C_{nn} & \mathbf{X}'_{\mathbf{s}_n} \\ \mathbf{X}_{\mathbf{s}_1} & \cdots & \mathbf{X}_{\mathbf{s}_n} & \mathbf{0} \end{pmatrix} \begin{pmatrix} \boldsymbol{\lambda} \\ \boldsymbol{\mu} \end{pmatrix} = \begin{pmatrix} C_{01} \\ \vdots \\ C_{0n} \\ \mathbf{X}_{\mathbf{s}_1^*} \end{pmatrix}, \quad (4)$$

where $C_{ij} = \text{Cov}(Y_{\mathbf{s}_i}(t), Y_{\mathbf{s}_j}(t))$ denotes the trace-covariogram function and $\boldsymbol{\mu} \in \mathbb{R}^L$ represents the Lagrange multiplier corresponding to the L unbiasedness constraints in (3). The UK approaches described above can be implemented through the publicly available R package `fdagstat` (Grujic and Menafoglio, 2017).

Although UK methods are valuable for exploratory data analysis, they are not based on formal statistical inference. The fitted results from the trace-covariogram function are plugged into (2) by ignoring the uncertainties in the estimation step. In terms of the model, the drift term in (1) is limited to the scalar covariates; therefore, we cannot study the relationships between functional variables. Furthermore, the uncertainty quantification of regression functions is not trivial for UK approaches. To address these challenges, we propose Bayesian spatial functional regression methods in the following section.

3 Functional Regression for Spatial Data

Let $Y_{\mathbf{s}_1}(t), \dots, Y_{\mathbf{s}_n}(t)$ be the observed functional response from a second-order stochastic process $\{Y_{\mathbf{s}}(t), t \in \mathcal{T}, \mathbf{s} \in \mathcal{D}\}$ in $\mathcal{L}^2(\mathcal{T})$. Similarly, we can define $X_{\mathbf{s}_1}(r), \dots, X_{\mathbf{s}_n}(r)$ as the observed functional covariates from a second-order stochastic process $\{X_{\mathbf{s}}(r), r \in \mathcal{V}, \mathbf{s} \in \mathcal{D}\}$ in $\mathcal{L}^2(\mathcal{V})$. To account for the spatial dependence between curves, we introduce a zero-mean Gaussian process $\{W_{\mathbf{s}}(t), t \in \mathcal{T}, \mathbf{s} \in \mathcal{D}\}$ that belongs to $\mathcal{L}^2(\mathcal{T})$. Here, we propose the spatial function-on-function regression (SFoFR) as

$$Y_{\mathbf{s}_i}(t) = \int_{\mathcal{V}} \Psi(r, t) X_{\mathbf{s}_i}(r) dr + W_{\mathbf{s}_i}(t) + \epsilon_{\mathbf{s}_i}(t), \quad (5)$$

where $\epsilon_{\mathbf{s}_i}(t)$ is an independent error function. The functional parameter (regression function) Ψ belongs to $\mathcal{L}(\mathcal{V}) \otimes \mathcal{L}(\mathcal{T})$, where \otimes indicates a tensor product. By extending the standard spatial regression models, SFoFR can study the relationships between functional variables and interpolate functions at unobserved locations. Following Kowal and Bourgeois (2020), we expand the functional variables in (5) with respect to the orthonormal basis functions $\{\phi_k\}_{k \in \mathbb{N}} \in \mathcal{L}(\mathcal{T})$, $\{\phi_g\}_{g \in \mathbb{N}} \in \mathcal{L}(\mathcal{V})$. For instance, we can orthonormalize the basis functions through QR factorization or directly use orthonormal ones (e.g., FPC, Fourier). Then, we have

$$Y_{\mathbf{s}_i}(t) = \sum_{k=1}^{\infty} y_{ik} \phi_k(t), \quad X_{\mathbf{s}_i}(r) = \sum_{g=1}^{\infty} x_{ig} \phi_g(r), \quad W_{\mathbf{s}_i}(t) = \sum_{k=1}^{\infty} w_{ik} \phi_k(t), \quad \epsilon_{\mathbf{s}_i}(t) = \sum_{k=1}^{\infty} e_{ik} \phi_k(t). \quad (6)$$

We can also construct the orthonormal tensor basis $\{\phi_{gk}\}_{g,k \in \mathbb{N}} = \{\phi_g\}_{g \in \mathbb{N}} \otimes \{\phi_k\}_{k \in \mathbb{N}} \in \mathcal{L}(\mathcal{V}) \otimes \mathcal{L}(\mathcal{T})$ and the regression function can be represented as

$$\Psi(r, t) = \sum_{k=1}^{\infty} \sum_{g=1}^{\infty} \psi_{gk} \phi_{gk}(r, t). \quad (7)$$

In (6), $\{y_{ik}\}_{k \in \mathbb{N}}$, $\{x_{ig}\}_{g \in \mathbb{N}}$, and $\{w_{ik}\}_{k \in \mathbb{N}}$ are correlated random variables across different spatial locations. Without loss of generality, we assume that they have mean zero and satisfy spatial homoscedasticity (Pineda-Ríos et al., 2019; Kang et al., 2023). We assume that the error coefficients $\{e_{ik}\}_{k \in \mathbb{N}}$ follow $\mathcal{N}(0, \tau^2)$ independently.

There are computational and inferential challenges for the model specified above. Since each functional component is correlated in terms of both t (within-curve dependence) and \mathbf{s}_i (between-curve dependence), we need to model covariance functions, resulting in complex likelihood functions. To address this, we utilize a basis transformation approach (Zhang et al., 2016; Kowal and Bourgeois, 2020). We transform each observed curve from the data space to the basis space and fit the model in the basis space. Then, we transform it back to the data space; the estimation and prediction results are interpreted in the data space. From this procedure, we can fit the model with a simpler covariance in the basis space while still modeling complex between and within-curve covariances in the data space. To transform to the basis space, we first take

the inner product with $\phi_{k'}(t)$ on both sides of (5) as

$$\int_{\mathcal{T}} \phi_{k'}(t) Y_{\mathbf{s}_i}(t) dt = \int_{\mathcal{T}} \phi_{k'}(t) \int_{\mathcal{V}} \Psi(r, t) X_{\mathbf{s}_i}(r) dr dt + \int_{\mathcal{T}} \phi_{k'}(t) W_{\mathbf{s}_i}(t) dt + \int_{\mathcal{T}} \phi_{k'}(t) \epsilon_{\mathbf{s}_i}(t) dt. \quad (8)$$

Since $\{\phi_k\}_{k \in \mathbb{N}}$ is an orthonormal basis function, using dominated convergence, the left-hand side of (8) becomes

$$\int \phi_{k'}(t) Y_{\mathbf{s}_i}(t) dt = \int \phi_{k'}(t) \left(\sum_{k=1}^{\infty} y_{ik} \phi_k(t) \right) dt = \sum_{k=1}^{\infty} y_{ik} \left(\int \phi_{k'}(t) \phi_k(t) dt \right) = y_{ik}, \quad (9)$$

when $k = k'$. In a similar fashion, $\int_{\mathcal{T}} \phi_k(t) W_{\mathbf{s}_i}(t) dt$ and $\int_{\mathcal{T}} \phi_k(t) \epsilon_{\mathbf{s}_i}(t) dt$ terms can be represented as w_{ik} and e_{ik} , respectively. Lastly, with dominated convergence, we have

$$\begin{aligned} \int_{\mathcal{T}} \phi_{k'}(t) \int_{\mathcal{V}} \Psi(r, t) X_{\mathbf{s}_i}(r) dr dt &= \int_{\mathcal{T}} \phi_{k'}(t) \int_{\mathcal{V}} \left(\sum_{k=1}^{\infty} \sum_{g=1}^{\infty} \psi_{gk} \phi_{gk}(r, t) \right) \left(\sum_{g=1}^{\infty} x_{ig} \phi_g(r) \right) dr dt \\ &= \sum_{g=1}^{\infty} \psi_{gk} x_{ig}, \end{aligned} \quad (10)$$

when $k = k'$. In practice, we approximate the above infinite basis expansions with the finite number of basis functions k_n and g_n , where k_n and g_n increase as $n \rightarrow \infty$ (Müller and Stadtmüller, 2005). Under this finite approximation, if we repeat (9), (10) with different k' , we have matrices of the coefficients in the basis space. Let $\tilde{\mathbf{Y}} = (y_{ik})_{n \times k_n}$ be the matrix of transformed curves in the basis space and $\tilde{\mathbf{X}} = (x_{ig})_{n \times g_n}$ be the design matrix with the coefficients $\tilde{\boldsymbol{\psi}} = (\psi_{gk})_{g_n \times k_n}$. Similarly, let $\tilde{\mathbf{W}} = (w_{ik})_{n \times k_n}$ be the transformed random effects matrix and $\tilde{\boldsymbol{\epsilon}} = (e_{ik})_{n \times k_n}$ be the transformed error matrix. Then, we can represent the SFoFR in the basis space with finite truncation as

$$\tilde{\mathbf{Y}} = \tilde{\mathbf{X}} \tilde{\boldsymbol{\psi}} + \tilde{\mathbf{W}} + \tilde{\boldsymbol{\epsilon}}, \quad (11)$$

where $\tilde{\mathbf{W}} \sim \mathcal{MG}\mathcal{P}(\boldsymbol{\Lambda}, \tilde{\boldsymbol{\Sigma}})$. Here, $\boldsymbol{\Lambda}$ is a between-curve covariance and $\tilde{\boldsymbol{\Sigma}}$ is a within-curve covariance (Morris and Carroll, 2006). (1) For continuous domains, we can use the Matérn class (Stein, 2012) covariance to model $\boldsymbol{\Lambda}$ that depends on the variance parameter σ^2 and range parameter ρ . (2) For discrete domains, we can use intrinsic autoregressive models (Besag and Kooperberg, 1995). Let $\mathbf{D} \in \mathbb{R}^{n \times n}$ be an adjacency matrix, where $D_{ij} = 1$, if locations i, j

are neighbors, and otherwise $D_{ij} = 0$. Then the model is defined with a precision matrix $\nu[\text{diag}(\mathbf{D}\mathbf{1}) - \mathbf{D}]$, where ν is a spatial smoothness parameter. For both continuous and discrete domains, we can model $\tilde{\Sigma}$ through a simple diagonal matrix in the basis space (e.g., $\tilde{\Sigma} = s\mathbf{I}$). Such an independence assumption in the basis space is justified for a wide variety of basis functions (Zhang et al., 2016). Note that while we use a simple covariance structure for $\tilde{\Sigma}$ in the basis space, it still allows a flexible covariance structure in the data space. In the following paragraph, we provide more details about the within-curve covariance in the data space.

Once we specify the priors of the parameters in (11), we can construct the MCMC algorithm to generate posterior samples from the basis space model. We provide the conditional distributions for SFoFR in the supplementary material. These posterior samples will be transformed back into the data space for interpreting the regression function and kriging. Let $\Phi \in \mathbb{R}^{k_n \times n_t}$ be a matrix of basis functions $\phi_k(t)$ evaluated at n_t grid points over \mathcal{T} . Similarly, let $\Xi \in \mathbb{R}^{g_n \times n_v}$ be the matrix of basis functions $\phi_g(r)$ evaluated at n_v grid points over \mathcal{V} . If we multiply both sides of (11) with Φ , we can transform back into the data space as

$$\tilde{\mathbf{Y}}\Phi = \tilde{\mathbf{X}}\Xi\Xi'\tilde{\psi}\Phi + \tilde{\mathbf{W}}\Phi + \tilde{\epsilon}\Phi.$$

The left-hand side term $\tilde{\mathbf{Y}}\Phi$ is a finite basis expansion of the observed curves evaluated over n_t grid points, which can be defined as $\mathbf{Y} \in \mathbb{R}^{n \times n_t}$. Similarly, $\tilde{\mathbf{X}}\Xi$, $\Xi'\tilde{\psi}\Phi$, $\tilde{\mathbf{W}}\Phi$, and $\tilde{\epsilon}\Phi$ can be defined as $\mathbf{X} \in \mathbb{R}^{n \times n_v}$, $\psi \in \mathbb{R}^{n_v \times n_t}$, $\mathbf{W} \in \mathbb{R}^{n \times n_t}$, and $\epsilon \in \mathbb{R}^{n \times n_t}$, respectively, which are finite representations of the functional components in (5). Then we have the SFoFR in the data space with finite truncation as

$$\mathbf{Y} = \mathbf{X}\psi + \mathbf{W} + \epsilon, \quad (12)$$

where $\mathbf{W} \sim \mathcal{MG}\mathcal{P}(\mathbf{A}, \Sigma)$. Therefore, in the data space, we allow a flexible form of the within-curve covariance as $\Sigma = \Phi'\tilde{\Sigma}\Phi$, while the MCMC algorithms are implemented in the basis space with a simple covariance structure as in (11). From $\psi = \Xi'\tilde{\psi}\Phi$, we can also interpret the regression function in the data space. A graphical description of the basis transformation approach is presented in Figure 1.

However, implementing the MCMC algorithm for (11) can still be computationally demanding

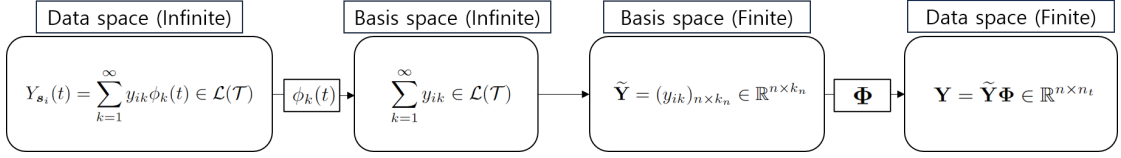


Figure 1: Outline of the basis transformation approach.

with increasing numbers of observations. The dimension of the transformed random effects $\tilde{\mathbf{W}} \in \mathbb{R}^{n \times k_n}$ becomes larger with larger n , and they are spatially correlated; this can lead to the slow mixing of the chain (Kang et al., 2023). To address this, we develop a projection-based SFoFR that is computationally efficient.

3.1 Projection-Based Function-on-Function Regression

Projection methods (Hughes and Haran, 2013; Lee and Haran, 2022) have been studied for both areal and point-level data for efficient computation. They can reduce the dimension of the spatial latent process from n to p ($\ll n$) based on the projection matrix $\mathbf{P} \in \mathbb{R}^{n \times p}$. Here, we apply these methods to the transformed random effect $\tilde{\mathbf{W}}$ in (11).

For the areal data over the discrete spatial domain, we construct the projection matrix \mathbf{P} by taking the leading p eigencomponents of Moran’s operator. Its eigenvalues correspond to the degree of spatial dependence, and the corresponding eigenvectors present the spatial clustering patterns of the data exhibit (Griffith, 2004; Hughes and Haran, 2013). To obtain \mathbf{P} , we first calculate \mathbf{H}^\perp which is a complement of $\mathbf{H} = \tilde{\mathbf{X}}(\tilde{\mathbf{X}}'\tilde{\mathbf{X}})^{-1}\tilde{\mathbf{X}}'$. Here, $\tilde{\mathbf{X}} \in \mathbb{R}^{n \times g_n}$ is a design matrix in (11). Then we calculate Moran’s operator $\mathbf{H}^\perp \mathbf{D} \mathbf{H}^\perp$, where $\mathbf{D} \in \mathbb{R}^{n \times n}$ is an adjacency matrix for observations. We take the leading p eigenvectors of Moran’s operator to construct $\mathbf{P} \in \mathbb{R}^{n \times p}$ and the transformed random effect $\tilde{\mathbf{W}}$ in (11) can be approximated as $\mathbf{P}\delta$.

For point-level data over the continuous spatial domain, we follow Lee and Haran (2022) to construct the projection matrix \mathbf{P} . First, we generate triangular mesh covering the spatial domain \mathcal{D} using the R package INLA (Lindgren and Rue, 2015). The mesh constructs an undirected graph $\mathbf{G} = (\mathbf{V}, E)$ where $\mathbf{V} = \{\mathbf{v}_1, \dots, \mathbf{v}_m\}$ is the set of locations of the mesh vertices and E is the set of edges. Then, we construct Moran’s operator $(\mathbf{I} - \mathbf{1}\mathbf{1}'/m)\mathbf{N}(\mathbf{I} - \mathbf{1}\mathbf{1}'/m)$, where $\mathbf{N} \in \mathbb{R}^{m \times m}$ is the adjacency matrix from the graph \mathbf{G} . As in the discrete case, we take the leading p eigenvectors

of Moran's operator to obtain $\mathbf{M} \in \mathbb{R}^{m \times p}$. Note that the eigenvectors present spatial dependence among the mesh vertices, not about point-level observations (Lee and Haran, 2022). Therefore, to interpolate observations within the mesh, we use piecewise linear basis functions $\mathbf{A} \in \mathbb{R}^{n \times m}$. The rows of \mathbf{A} correspond to the observed locations, and the columns correspond to the mesh vertices; the i -th row of \mathbf{A} contains weights to interpolate onto point-level locations. From this, we can construct a projection matrix $\mathbf{P} = \mathbf{A}\mathbf{M} \in \mathbb{R}^{n \times p}$ and approximate the transformed random effect $\widetilde{\mathbf{W}}$ in (11) as $\mathbf{P}\boldsymbol{\delta}$.

Therefore, for both discrete and continuous domains, we have the projection-based SFoFR (PSFoFR) in the basis space as

$$\widetilde{\mathbf{Y}} = \widetilde{\mathbf{X}}\widetilde{\boldsymbol{\psi}} + \mathbf{P}\boldsymbol{\delta} + \widetilde{\boldsymbol{\epsilon}}. \quad (13)$$

As in SFoFR, we use the MCMC algorithm to sample from the posterior distributions in the basis space model (13) and transform them back into the data space for inference. We provide the details about the full conditionals for PSFoFR in the supplementary material.

For the point-level data, predictions at unobserved locations (i.e., kriging) are of great interest. Consider we have n_{cv} number of unobserved locations $\mathbf{s}^* = (\mathbf{s}_1^*, \dots, \mathbf{s}_{n_{cv}}^*) \in \mathcal{D}$. Similar to (6), let $\widetilde{\mathbf{Y}}_{\mathbf{s}^*} = (y_{ik})_{n_{cv} \times k_n}$ and $\widetilde{\mathbf{X}}_{\mathbf{s}^*} = (x_{ig})_{n_{cv} \times g_n}$ be the matrices of basis coefficients obtained from response curves and covariate curves at \mathbf{s}^* , respectively. For PSFoFR, we can construct a piecewise linear basis function matrix $\mathbf{A}_{\mathbf{s}^*} \in \mathbb{R}^{n_{cv} \times m}$, where the i -th row of $\mathbf{A}_{\mathbf{s}^*}$ contains weights to interpolate the vertices onto \mathbf{s}^* . As before, we can obtain a projection matrix $\mathbf{P}_{\mathbf{s}^*} = \mathbf{A}_{\mathbf{s}^*}\mathbf{M} \in \mathbb{R}^{n_{cv} \times p}$. From this, the linear predictor $\widetilde{\boldsymbol{\eta}}_{\mathbf{s}^*} \in \mathbb{R}^{n_{cv} \times k_n}$ at the basis space is defined as

$$\widetilde{\boldsymbol{\eta}}_{\mathbf{s}^*} = \widetilde{\mathbf{X}}_{\mathbf{s}^*}\widetilde{\boldsymbol{\psi}} + \mathbf{P}_{\mathbf{s}^*}\boldsymbol{\delta}. \quad (14)$$

For interpretation, we transform it back to the data space by multiplying $\boldsymbol{\Phi}$ at both sides of (14) as

$$\boldsymbol{\eta}_{\mathbf{s}^*} = \widetilde{\boldsymbol{\eta}}_{\mathbf{s}^*}\boldsymbol{\Phi} = \widetilde{\mathbf{X}}_{\mathbf{s}^*}\boldsymbol{\Xi}\boldsymbol{\Xi}'\widetilde{\boldsymbol{\psi}}\boldsymbol{\Phi} + \mathbf{P}_{\mathbf{s}^*}\boldsymbol{\delta}\boldsymbol{\Phi}. \quad (15)$$

For the given posterior samples, we obtain a posterior predictive distribution of $\boldsymbol{\eta}_{\mathbf{s}^*} \in \mathbb{R}^{n_{cv} \times n_t}$ from (15).

3.2 Theoretical Justifications

Consider the PSFoFR with the following representations.

1. Let $\Psi \in \mathcal{L}(\mathcal{V}) \otimes \mathcal{L}(\mathcal{T})$ be the true regression function in the data space defined as $\Psi = \sum_{k=1}^{\infty} \sum_{g=1}^{\infty} \psi_{gk} \phi_{gk}$.
2. Let $\Psi_{g_n k_n} = \sum_{k=1}^{k_n} \sum_{g=1}^{g_n} \psi_{gk} \phi_{gk}$ be the truncated regression function in the data space with large enough g_n and k_n so that $\sum_{k>k_n} \sum_{g>g_n} \psi_{gk} \phi_{gk}$ is negligible. And let $\tilde{\Psi}_{g_n k_n} = \begin{pmatrix} \psi_{11} & \cdots & \psi_{1k_n} \\ \vdots & \ddots & \vdots \\ \psi_{g_n 1} & \cdots & \psi_{g_n k_n} \end{pmatrix}$.
3. Let $\tilde{\Psi}_{g_n k_n}^{(u)} = \begin{pmatrix} \psi_{11}^{(u)} & \cdots & \psi_{1k_n}^{(u)} \\ \vdots & \ddots & \vdots \\ \psi_{g_n 1}^{(u)} & \cdots & \psi_{g_n k_n}^{(u)} \end{pmatrix}$ be the posterior sample from u th iteration of MCMC.
4. Let $\Psi_{g_n k_n}^{(u)} = \sum_{k=1}^{k_n} \sum_{g=1}^{g_n} \psi_{gk}^{(u)} \phi_{gk} \in \mathcal{L}(\mathcal{V}) \otimes \mathcal{L}(\mathcal{T})$ be a function constructed using MCMC samples.
5. Let $\hat{\Psi}_{g_n k_n}^{(u)} = \sum_{k=1}^{k_n} \sum_{g=1}^{g_n} \hat{\psi}_{gk}^{(u)} \phi_{gk}$ be the estimated regression function where $\hat{\psi}_{gk}^{(u)} = \frac{1}{u} \sum_{l=1}^u \psi_{gk}^{(l)}$.
And let $\hat{\Psi}_{g_n k_n}^{(u)} = \begin{pmatrix} \hat{\psi}_{11}^{(u)} & \cdots & \hat{\psi}_{1k_n}^{(u)} \\ \vdots & \ddots & \vdots \\ \hat{\psi}_{g_n 1}^{(u)} & \cdots & \hat{\psi}_{g_n k_n}^{(u)} \end{pmatrix}$.

Assumption 3.1. *The presumptions are summarized as follows.*

1. *The basis systems $\{\phi_g\}_{g=1}^{\infty}$ and $\{\phi_k\}_{k=1}^{\infty}$ are fixed orthonormal system of $\mathcal{L}(\mathcal{V})$ and $\mathcal{L}(\mathcal{T})$.
From this, we can a construct tensor basis system $\{\phi_{gk}\}_{g,k=1}^{\infty} \in \mathcal{L}(\mathcal{V}) \otimes \mathcal{L}(\mathcal{T})$.*
2. *The truncation $k_n \rightarrow \infty$ as $n \rightarrow \infty$, and truncation $g_n \rightarrow \infty$ as $n \rightarrow \infty$.*
3. *$\Psi, \Psi_{g_n k_n}, \Psi_{g_n k_n}^{(u)}$, and $\hat{\Psi}_{g_n k_n}^{(u)}$ are defined on the same probability space.*

Assumption 3.1 is not restrictive. The first assumption is that we are working under a given fixed tensor product basis system defined in $\mathcal{L}(\mathcal{V}) \otimes \mathcal{L}(\mathcal{T})$. In the second assumption,

k_n , g_n depends on n , and both go to infinity when n goes to infinity, which is commonly assumed. The third assumption is for implementing computation on these functions. Note that $\|\cdot\|$ denotes the norm in $\mathcal{L}(\mathcal{V}) \otimes \mathcal{L}(\mathcal{T})$, and $\|\cdot\|_{\mathbb{R}^{g_n \times k_n}}$ is the norm in $\mathbb{R}^{g_n \times k_n}$. Under these assumptions, Theorem 3.1 shows that the function obtained through the MCMC algorithm converges in distribution to the true function. From this, we can construct the corresponding credible intervals in Section 3.3.

Theorem 3.1. *Consider the sequence of random functions $\{\Psi_{g_n k_n}^{(u)}\}_{n,u} \in \mathcal{L}(\mathcal{V}) \otimes \mathcal{L}(\mathcal{T})$. Then, $\Psi_{g_n k_n}^{(u)} \xrightarrow{D} \Psi$ as $n \rightarrow \infty$ and $u \rightarrow \infty$.*

Proof. In terms of the total variation distance, an ergodic Markov chain $\{\tilde{\psi}_{gk}^{(u)}\}_{u \in \mathbb{N}}$ converges to the stationary posterior distribution $\pi(\tilde{\psi}|\mathbf{Y})$. Therefore, we have $\tilde{\psi}_{g_n k_n}^{(u)} \xrightarrow{D} \tilde{\psi}_{g_n k_n}$ as $u \rightarrow \infty$ for every g_n and $k_n \in \mathbb{N}$. Then, by the continuous mapping theorem $\Psi_{g_n k_n}^{(u)} \xrightarrow{D} \Psi_{g_n k_n}$ for every g_n and k_n . Since $\Psi_{g_n k_n} \xrightarrow{D} \Psi$ as $n \rightarrow \infty$, we have $\Psi_{g_n k_n}^{(u)} \xrightarrow{D} \Psi$ as $n \rightarrow \infty$ and $u \rightarrow \infty$. ■

Theorem 3.2 shows that the estimated regression function $\widehat{\Psi}_{g_n k_n}^{(u)}$ converges in probability to the true regression function Ψ as the n (sample size) and u (MCMC sample size) go to infinity.

Theorem 3.2. *Consider the estimated regression function $\widehat{\Psi}_{g_n k_n}^{(u)}$. Under aforementioned assumptions, we have $\widehat{\Psi}_{g_n k_n}^{(u)} \xrightarrow{P} \Psi$ as $n \rightarrow \infty$ and $u \rightarrow \infty$.*

Proof. First, we fix g_n and k_n . Since $\{\tilde{\psi}_{gk}^{(u)}\}_{u \in \mathbb{N}}$ is an ergodic and stationary Markov chain, we have $\widehat{\psi}_{g_n k_n} \xrightarrow{P} \tilde{\psi}_{g_n k_n}$ as $u \rightarrow \infty$ by the weak law of large numbers. As

$$P(\|\Psi_{g_n k_n}^{(u)} - \Psi_{g_n k_n}\|^2 \geq \frac{\epsilon}{2}) = P(\|\widehat{\psi}_{g_n k_n} - \tilde{\psi}_{g_n k_n}\|_{\mathbb{R}^{g_n \times k_n}}^2 \geq \frac{\epsilon}{2}) \rightarrow 0,$$

we have $\Psi_{g_n k_n}^{(u)} \xrightarrow{P} \Psi_{g_n k_n}$ as $u \rightarrow \infty$ for every $g_n, k_n \in \mathbb{N}$. Since $\Psi_{g_n k_n}$ is truncated version of Ψ , we have $\Psi_{g_n k_n} \xrightarrow{P} \Psi$ as $n \rightarrow \infty$ (i.e. $g_n, k_n \rightarrow \infty$), resulting in $P(\|\Psi_{g_n k_n} - \Psi\|^2 \geq \frac{\epsilon}{2}) \rightarrow 0$.

Then,

$$\begin{aligned}
P(\|\Psi_{g_n k_n}^{(u)} - \Psi\|^2 \geq \epsilon) &\leq P(\|\Psi_{g_n k_n}^{(u)} - \Psi_{g_n k_n}\|^2 + \|\Psi_{g_n k_n} - \Psi\|^2 \geq \epsilon) \\
&\leq P(\|\Psi_{g_n k_n}^{(u)} - \Psi_{g_n k_n}\|^2 \geq \frac{\epsilon}{2}) + P(\|\Psi_{g_n k_n} - \Psi\|^2 \geq \frac{\epsilon}{2}) \\
&\rightarrow 0 + 0.
\end{aligned}$$

as $n \rightarrow \infty$ and $u \rightarrow \infty$. ■

3.3 Simultaneous Credible Intervals for Functional Parameters

Following Meyer et al. (2015), we calculate the simultaneous credible intervals for the regression function. First, we construct a set of functions $\left\{ \Psi_{g_n k_n}^{(l)}(r, t) = \sum_{k=1}^{k_n} \sum_{g=1}^{g_n} \psi_{gk}^{(l)} \phi_{gk}(r, t) \right\}_{l=1}^u$ from the MCMC samples $\left\{ \tilde{\psi}_{g_n k_n}^{(l)} \right\}_{l=1}^u$ obtained from the posterior distribution. We evaluate the $\Psi_{g_n k_n}^{(u)}(r, t)$ for each time point $r = 1, \dots, n_v$ and $t = 1, \dots, n_t$, where $1 < 2 < \dots < n_v$ and $1 < 2 < \dots < n_t$, respectively. Let M_α be the $(1 - \alpha)$ sample quantile of

$$Z^{(u)} = \max_{1 \leq r \leq n_v, 1 \leq t \leq n_t} \left| \frac{\Psi_{g_n k_n}^{(u)}(r, t) - \widehat{\Psi}_{g_n k_n}^{(u)}(r, t)}{\text{SD}(\Psi_{g_n k_n}(r, t))} \right|,$$

where $\widehat{\Psi}_{g_n k_n}^{(u)}(r, t)$ and $\text{SD}(\Psi_{g_n k_n}(r, t))$ be the sample mean and sample standard deviation of $\Psi_{g_n k_n}^{(u)}(r, t)$, respectively. Then, $(1 - \alpha)$ simultaneous credible intervals can be obtained as

$$I(\alpha, r, t) = \widehat{\Psi}_{g_n k_n}^{(u)}(r, t) \pm M_\alpha \text{SD}(\Psi_{g_n k_n}(r, t)).$$

To detect the significant region of the regression function, we also compute Simultaneous Band Scores (SimBaS) (Meyer et al., 2015) by converting simultaneous intervals. As in Meyer et al. (2015), we first construct $I(\alpha, r, t)$ for multiple levels of α . Then, for each (r, t) , we determine the minimum α at which each $I(\alpha, r, t)$ excludes zero (i.e., $P_{\text{SimBaS}}(r, t) = \min\{\alpha : 0 \notin I(\alpha, r, t)\}$). SimBas can be computed as

$$P_{\text{SimBaS}}(r, t) = \frac{1}{u} \sum_{l=1}^u 1 \left\{ \left| \frac{\widehat{\Psi}_{g_n k_n}^{(l)}(r, t)}{\text{SD}(\Psi_{g_n k_n}(r, t))} \right| \leq Z^{(l)} \right\}.$$

Here, we can specify the level α and identify the significant region (r, t) that satisfies $P_{\text{SimBas}}(r, t) < \alpha$. This is equivalent to checking whether $I(\alpha, r, t)$ covers zero at a chosen α -level.

4 Simulation Study

In this section, we apply the proposed method to simulated spatial functional datasets. To represent the performance of PSFoFR, we compare it with FoFR (i.e., independent model), SFoFR and standard UK. We implement PSFoFR, SFoFR, and FoFR in `nimble` (de Valpine et al., 2017), and implement UK through R package `fdagstat` (Grujic and Menafoglio, 2017). We show the main results with B-spline basis functions and provide fitted results using the Fourier and FPC basis functions in the supplementary material. We run MCMC algorithms until the Monte Carlo standard errors (Jones et al., 2006; Flegal et al., 2008) for PSFoFR are at or below 0.04 (70,000 iterations). All codes were run on 16-core AMD Ryzen 9 7950X processors. The source code can be downloaded from <https://github.com/codinheesang/PSFoFR>. The simulation procedures are summarized as follows.

1. We simulate 1,000 locations in the $\mathcal{D} = [0, 1]^2$ domain. For each location, we generate $\{x_{ig}\}_{1,000 \times 15}$ from a normal distribution with the mean as the x -axis of the location and a variance of 1. By using 15 B-spline basis functions, we create $X_{\mathbf{s}_i}(r) = \sum_{g=1}^{15} x_{ig} \phi_g(r)$ for $i = 1, \dots, 1,000$.
2. Then we generate $\{w_{ik}\}_{1,000 \times 15}$ from a Gaussian process with a mean 0 and a Matérn covariance, where the distance matrix is calculated from the simulated locations. We use a variance 0.5, range 0.2, and a smoothness 0.5. Similarly, we create $W_{\mathbf{s}_i}(t) = \sum_{k=1}^{15} w_{ik} \phi_k(t)$ for $i = 1, \dots, 1,000$.
3. Following Meyer et al. (2015), we use the true regression function defined over the $[0, 225] \times [0, 225]$ domain as

$$\Psi(r, t) = \frac{7}{500} \frac{1}{\sqrt{0.006\pi}} \exp \left[-\frac{1}{0.006} \left(\frac{t-r}{225} \right)^2 \right].$$

Then, from the finite basis expansion $\Psi(r, t) = \sum_{k=1}^{15} \sum_{g=1}^{15} \psi_{gk} \phi_{gk}(r, t)$, we obtain ψ_{gk} for $g, k = 1, \dots, 15$.

4. We simulate $\tilde{\mathbf{Y}} = (y_{ik})_{1,000 \times 15}$ from (11) and obtain $Y_{s_i}(t) = \sum_{k=1}^{15} y_{ik} \phi_k(t)$ for $i = 1, \dots, 1,000$. When we do not consider the measurement error, we simulate $\{y_{ik}\}_{1,000 \times 15}$ from $\tilde{\mathbf{Y}} = \tilde{\mathbf{X}}\tilde{\boldsymbol{\psi}} + \tilde{\mathbf{W}}$.

We use $n = 700$ samples for training and $n_{cv} = 300$ samples for prediction. For UK, we use a default Gaussian model for variogram fitting and plug in the simulated $\{x_{ig}\}_{n \times 15}$ as covariates; note that UK cannot directly model functional covariates. For PSFoFR, SFoFR, and FoFR, we run the MCMC algorithm for 70,000 iterations, with 50,000 discarded for burn-in, and 1,000 thinned samples obtained from the remaining 20,000. We choose the number of basis functions k_n and g_n by minimizing the generalized cross-validation (GCV) error. For PSFoFR, we use 1,520 triangular meshes to construct the projection matrix over the continuous spatial domain. We study PSFoFR with different rank values $p = 50, 100, 150$, corresponding to 5%, 10%, and 15% of the sample size. To assess the performance of the algorithms, we compare the mean square prediction error (MSPE) defined as $\sqrt{\frac{1}{n_{cv}n_t} \sum_{\forall s^*, t} (Y_{s^*}(t) - \hat{Y}_{s^*}(t))^2}$ with $n_t = 225$ grid points over the $[0, 225]$ domain. For functional regression models, we also compute the mean square error (MSE) of the regression function as $\sqrt{\frac{1}{n_t n_v} \sum_{\forall r, t} (\Psi(r, t) - \hat{\Psi}(r, t))^2}$ with $n_t \times n_v = 225 \times 225$ grid points over the $[0, 225] \times [0, 225]$ domain.

Model	MSPE	MSE	Time
PSFoFR ($p = 50$)	0.106	0.004	34
PSFoFR ($p = 100$)	0.099	0.004	39
PSFoFR ($p = 150$)	0.098	0.004	43
SFoFR	0.091	0.004	287
FoFR	0.182	0.004	19
UK	0.123	-	< 1

Table 1: Inference results for the simulated dataset. MSPE, MSE, and computing time (min) are reported.

Table 1 shows that functional regression approaches can accurately estimate $\Psi(r, t)$ with a small MSE, while UK cannot. Compared to SFoFR, PSFoFR is computationally much faster due to the projection step. The performance of PSFoFR is similar across different ranks. This

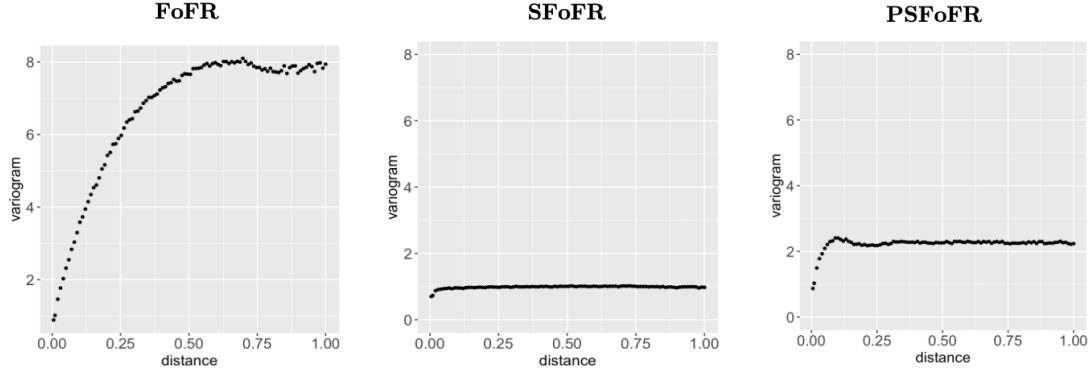


Figure 2: Fitted trace-variograms for the simulated datasets.

implies that choosing p as 5% to 10% of the samples can quickly provide accurate inference results, as suggested in Hughes and Haran (2013); Lee and Haran (2022). We observe that FoFR has the highest MSPE value. To analyze the correlation among residuals, we compute the trace-variogram through `fdagstat` package. Figure 2 indicates that residuals from FoFR are more correlated than those from PSFoFR and SFoFR.

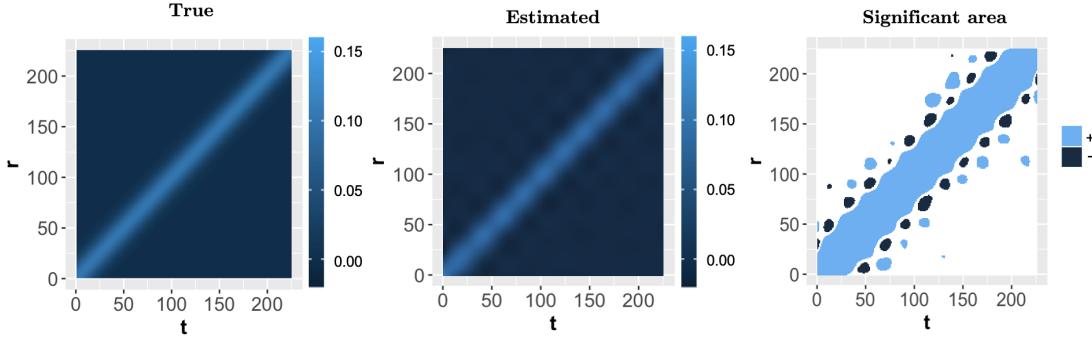


Figure 3: The estimated regression functions. Significant areas in the functions are detected from $\alpha = 0.05$. Sky blue colors represent positive significant areas, whereas dark blue colors represent negative significant areas.

Here, we visualize the inference results from PSFoFR with $p = 50$ since the results from other rank choices are quantitatively similar. Figure 3 indicates that the estimated regression functions from PSFoFR are similar to the true regression function. Furthermore, the significant areas detected from the 95% simultaneous credible intervals and SimBas are well aligned with the important regions of the true function. Note that UK approaches cannot quantify such relationships between functional variables.

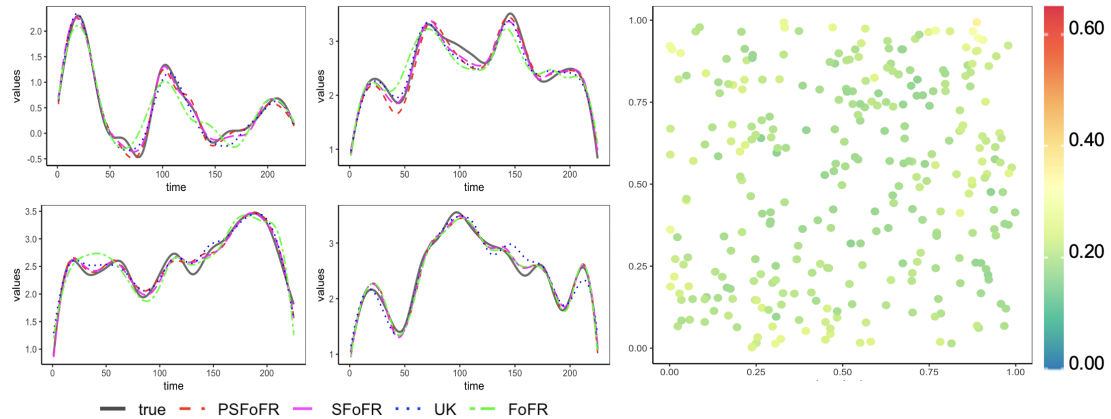


Figure 4: Visualizations of predicted curves (left panel) and prediction uncertainties (right panel) for both cases.

Figure 4 provides four predicted curves from 300 test observations. All methods can capture the trend of the true response functions, while FoFR shows slight differences, which are aligned with the results in Table 1. Figure 4 also visualizes the prediction uncertainties for each spatial location. We calculate the length of the 95% credible intervals for every time grid and compute the mean of them for each test spatial location. In general, prediction uncertainties are larger at the boundaries of the region, which are more difficult to predict due to a lack of neighboring information.

5 Application

In this section, we apply our methods to two real data examples with spatial functional variables: (1) PM2.5 data (continuous domain) and (2) mobility data (discrete domain). For both cases, the proposed approach can estimate regression functions and detect the significant region of the estimated functions. Furthermore, our method can provide more (or comparable) accurate kriging results than UK in the point-level data example (PM 2.5 data).

5.1 PM2.5 Data

Particle pollution from fine particulates (PM2.5) is a crucial indicator of air quality. Long-term exposure to PM2.5 can increase the risk of health problems, such as heart disease, low birth

weight, and asthma. Note that PM2.5 is influenced by various environmental factors, meteorological conditions, and other pollutant emissions. It is well known that anthropogenic emissions of nitrogen oxides (NOx) and carbon monoxide (CO) can affect PM2.5 concentrations on an intercontinental scale (Leibensperger et al., 2011). Especially, NOx emissions affect air quality since the reduction of NOx emission consecutively reduces NO_3^- and NH_4^+ which compose PM2.5 particles (Kang and Kim, 2022). Therefore, studying the functional relationship between PM2.5 and NOx would be useful for establishing public health policy. Furthermore, predicting PM2.5 curves for unobserved locations is crucial for public health management.

Here, we study the PM2.5 dataset collected from the Ministry of Environment Japan (Ministry of the Environment Government of Japan, 2023) observed at 991 monitoring stations. The dataset contains daily mean values of PM2.5 (January 20, 2024, to January 31, 2024) and NOx values (January 8, 2024, to January 19, 2024). We use the log PM2.5 values as a functional response and the NOx values as a functional covariate in the proposed model. The mean of the log PM2.5 and NOx curves are illustrated in the supplementary material. For UK, we use a default Gaussian model for the variogram fitting. For PSFoFR, we use $k_n = 11$ and $g_n = 11$ orthonormalized B-spline basis functions; the number of basis functions is chosen by minimizing the GCV error. To construct the projection matrix over the continuous spatial domain, we use 1,719 triangular meshes and set p as about 5% of the sample size (i.e., $p = 46$). We run MCMC algorithms until the Monte Carlo standard errors (Jones et al., 2006; Flegal et al., 2008) for PSFoFR are at or below 0.04 (50,000 iterations). We use 638 samples for training and the remaining 273 samples for validation. For PSFoFR, it takes 11.80 minutes for computation, while SFoFR takes 184.12 minutes, indicating that PSFoFR is computationally more efficient. FoFR takes about 5.8 minutes because the model does not consider spatial correlation. Compared to functional regression models, UK only takes about a second.

Figure 5 illustrates that the lower right corner parts of the estimated $\Psi(r, t)$ have high values, which implies that there is a positive relationship between NOx values and PM2.5 in the near term. Such a relationship becomes insignificant in the long term but only lasts for a few days. Specifically, it shows that the NOx values on January 18th have a positive relationship with PM2.5 levels from January 20th to January 23rd. This result coincides with the previous studies in Fu et al. (2023); Huang et al. (2024), which show that PM2.5 is NOx-sensitive and suggest

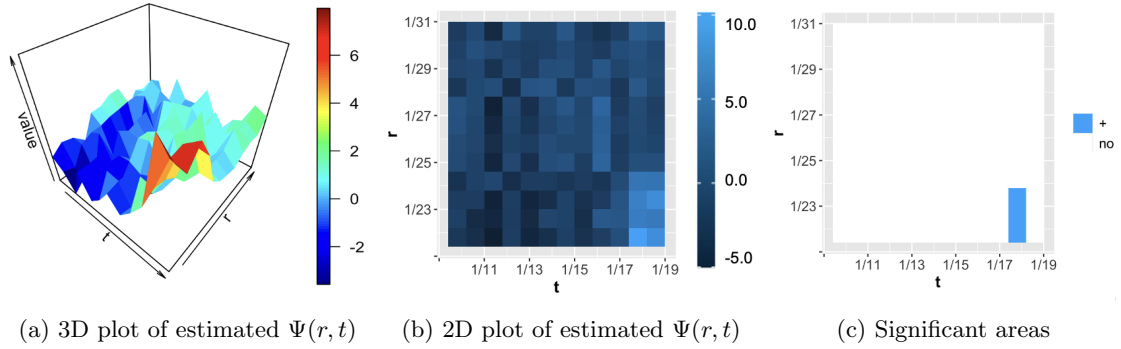


Figure 5: Japan PM2.5 data: Estimated $\Psi(r, t)$ from PSFoFR. Significant areas in the functions are detected from $\alpha = 0.05$. Sky blue colors represent positive significant areas, whereas dark blue colors represent negative significant areas.

that reducing NOx emissions has an impact on lowering PM2.5.

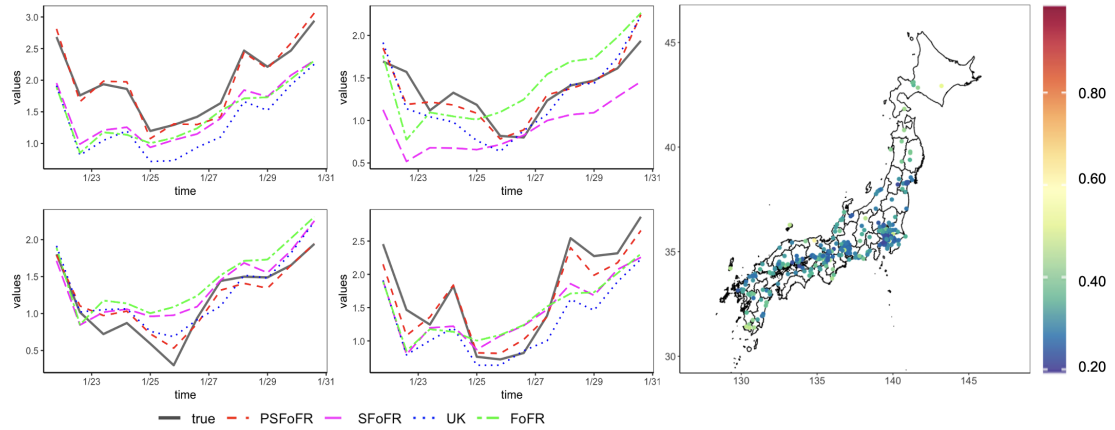


Figure 6: Visualizations of predicted curves (left panel) and prediction uncertainties (right panel) for Japan PM2.5 data.

Figure 6 provides functional kriging results from PSFoFR and UK at four locations among 273 test observations. We observe that our methods provide more accurate kriging performance than UK. The MSPE of PSFoFR, SFoFR, UK, and FoFR are 0.780, 0.823, 0.806, and 0.838, respectively. PSFoFR shows the lowest MSPE value, while FoFR has the highest MSPE value. The MSPE value from SFoFR is relatively high because high-dimensional random effects $\widetilde{\mathbf{W}}$ cause the poor mixing of the chains. The trace-variograms indicate that residuals from FoFR show a more distinct pattern compared to spatial models (Figure 7). As in the previous section, we also provide a prediction uncertainty map for PSFoFR (Figure 6). We observe that the

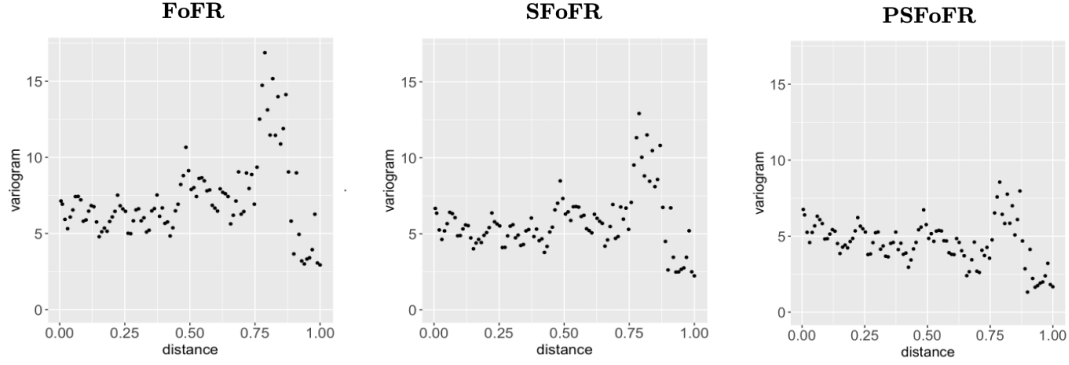


Figure 7: Fitted trace-variograms for the PM2.5 datasets.

uncertainties are larger for the region with fewer observations, which is natural.

5.2 Mobility Data

Population mobility counts the number of individuals in a specific area during a given period based on the location information obtained from mobile phone base stations. It encompasses the total count of the mobile population, accounting for time overlaps, which include both the population not moving within the area and the population actively moving within the area. This population mobility data is sourced from a major mobile service provider in South Korea, SK Telecom (SKT), which holds 40% of the total mobile telecommunication subscribers. The data is the form of origin-destination data, which has been preprocessed and expanded from the raw data to represent the entire population by adjusting the number of SKT users according to their market share in each region.

Data items are categorized by the daily outflow and inflow populations and segmented by gender, age group, and region. The “origin” is determined based on the previous month, specifically on the area where individuals spent the most time between 00:00 and 06:00. Based on this, individuals leaving the origin for other locations (destination) are defined as the outflow population, and those entering the origin location are defined as the inflow population. Geographic regions are divided into the city (Si), county (Gun), and district level (Gu), and the population count is based on individuals who have spent at least 2 hours in a specific area. If an individual visits multiple locations for over 2 hours daily, the same individual may be counted multiple

times. However, duplicate counts are excluded if the same individual visits the same area on the same day, on a daily basis.

In our analysis, we use 182 weekly mean values of total flow (outflow+inflow) populations from April 2019 to September 2022 by the areal unit as a functional response. We use the population pyramid of each region as a functional covariate, which is collected from KOSIS (https://kosis.kr/statHtml/statHtml.do?orgId=101&tblId=DT_1IN1509&conn_path=I2). The dataset contains the proportion of the 16 age groups (≤ 15 , 15-19, 20-24, 25-29, 30-34, 35-39, 40-44, 45-49, 50-54, 55-59, 60-64, 65-69, 70-74, 75-79, 80-84 ≥ 85) in 250 geographic regions, city (Si), county (Gun), and district (Gu) in 2022. We use the population mobility values as a functional response and the proportion of the age group as a functional covariate in the proposed model. For PSFoFR, we use $k_n = 19$ and $g_n = 10$ orthonormalized B-spline basis functions; the number of basis functions are chosen by minimizing the GCV error. To construct the projection matrix over the continuous spatial domain, we use $p = 24$, which is about 10% of the sample size. We run MCMC algorithms until the Monte Carlo standard errors (Jones et al., 2006; Flegal et al., 2008) for PSFoFR are at or below 0.04 (50,000 iterations). Both PSFoFR and SFoFR take about 30 minutes for the same iterations. However, to achieve the same Monte Carlo standard error criteria (0.04), SFoFR needs three times longer iterations, indicating that the mixing of the chain is slower than those from PSFoFR.

To analyze the spatial correlation among residuals, we use Moran's I (Moran, 1950), which is a commonly used exploratory method for areal data. For each time grid, we compute Moran's I values and average them. We observe that the averaged Moran's I values (p-values) are 0.000 (0.721), 0.162 (0.019), and 0.211 (0.002) for PSFoFR, SFoFR, and FoFR, respectively. PSFoFR can address the correlation in the data better than other methods, signified by the higher p-values.

Figure 8 shows the estimated regression function and its significant areas. We observe that the age groups 20-24 ($t = 3$) and 40-44 ($t = 7$) have a significant positive relationship with mobility in general. On the other hand, the age groups ≤ 15 ($t = 1$) and 80-84 ($t = 15$) have a significant negative relation with mobility. This implies that the regions with a high population of individuals in the 20-24 and 40-44 (≤ 15 and 80-84) age groups tend to record a high (low) mobility. However, we observe that a positive relationship between age group 20-24 with mobility

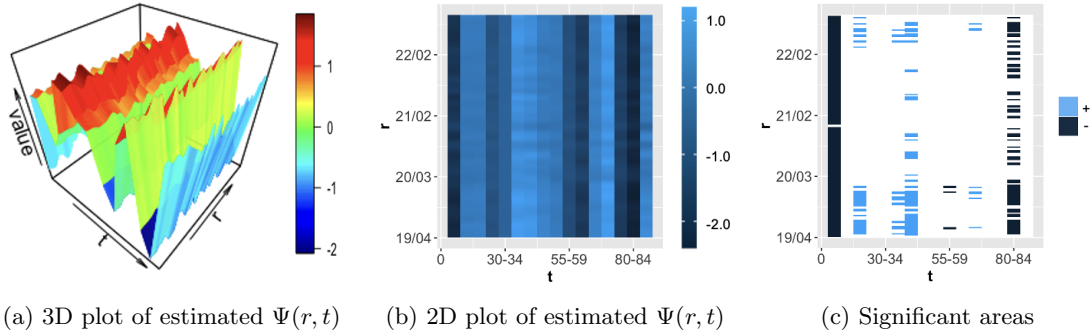


Figure 8: Korea Mobility data: Estimated $\Psi(r, t)$ from PSFoFR. Significant areas in the functions are detected from $\alpha = 0.05$. Sky blue colors represent positive significant areas, whereas dark blue colors represent negative significant areas.

is not significant from March 2020 to February 2022. The age group 40-44 also shows less significant relationships in that period. This is due to the social distancing policies implemented in South Korea from March 2020 to April 2022 (Ha et al., 2023). In that period, the mean of the mobility curves becomes lower than in other periods, which is illustrated in the supplementary material. The social distancing policy for COVID-19 control decreases overall mobility, resulting in a less significant relationship from March 2020 to February 2022.

6 Discussion

In this manuscript, we propose a Bayesian framework for FoFR in the presence of spatial correlation. We utilize the basis transformation and projection methods to address within-curve and between-curve dependencies in the model efficiently. By incorporating functional covariates into the model, both SFoFR and PSFoFR can show improved kriging performance and provide interpretations of regression functions. The proposed methods can also be applicable to the spatial functional data over discrete domains. We have also studied the convergence of the regression function with an increasing sample size and MCMC iteration. Uncertainty quantification in estimation and prediction through posterior samples is also one of the advantages over the existing method. PSFoFR is computationally more efficient than SFoFR and shows faster mixing of the chain, while they provide comparable inferential results.

The proposed framework is flexible and can be extendable to a wide variety of hierarchical

functional regression models. For example, we can consider additive function-on-function regressions (Kim et al., 2018) or non-Gaussian functional response models (Scheipl et al., 2016) for spatial functional data. Once the models include spatially dependent latent processes within the hierarchical model, we can readily use SFoFR or PSFoFR with minor changes to the `nimble` code. As per future research direction, one might consider different spatial basis functions to represent correlated \mathbf{W} . Examples include thin plate splines (Lee and Park, 2023), multi-resolution basis (Katzfuss, 2017), and predictive process (Banerjee et al., 2008). A closer examination of adopting different spatial basis functions can improve the performance of the proposed method.

Supplementary Material

Supplementary materials available online contain the full conditionals for MCMC, simulation studies with various basis functions, estimated regression functions from SFoFR, and mean trends of functional variables.

Acknowledgement

This work was supported by the National Research Foundation of Korea (2020R1C1C1A0100386814, RS-2023-00217705, 2021R1A2C1095639) and the ICAN (ICT Challenge and Advanced Network of HRD) support program (RS-2023-00259934) supervised by the IITP (Institute for Information & Communications Technology Planning & Evaluation). The authors are grateful to the anonymous reviewers for their careful reading and valuable comments.

Supplementary Material for Bayesian Function-on-Function Regression for Spatial Functional Data

Heesang Lee, Dagun Oh, Sunhwa Choi, and Jaewoo Park

A Full Conditionals for Markov Chain Monte Carlo

A.1 Full Conditionals for SFoFR

For continuous spatial domains, let $f(y_{ik}|\psi_{gk}, \widetilde{\mathbf{W}}, \tau^2, \Sigma_{\widetilde{\mathbf{W}}})$ be the normal likelihood function with priors $p(\psi_{gk}), p(\tau^2), p(\Sigma_{\widetilde{\mathbf{W}}})$ where $\Sigma_{\widetilde{\mathbf{W}}}$ is covariance structure of $\widetilde{\mathbf{W}}$. Then, we can define the joint posterior distribution for SFoFR (basis space) as $\pi(\psi_{gk}, \widetilde{\mathbf{W}}, \tau^2, \Sigma_{\widetilde{\mathbf{W}}}|y_{ik}) \propto f(y_{ik}|\psi_{gk}, \widetilde{\mathbf{W}}, \tau^2) f(\widetilde{\mathbf{W}}|\Sigma_{\widetilde{\mathbf{W}}})p(\psi_{gk})p(\tau^2)p(\Sigma_{\widetilde{\mathbf{W}}})$. Here, we use independent normal conjugate priors for $\psi_{gk} \sim \mathcal{N}(0, 10)$, inverse gamma conjugate priors for $\tau^2 \sim \mathcal{IG}(2, 0.1)$ and $\sigma^2 \sim \mathcal{IG}(2, 0.1)$, and a uniform prior for $\rho \sim \text{Unif}(0, 1)$. Let $\Sigma_{\widetilde{\mathbf{W}}} = \sigma^2\Gamma(\rho)$ be the Matérn class (Stein, 2012) covariance matrix with the range parameter ρ and variance σ^2 . Then, the full conditional distributions are derived as follows.

- The conditional distribution of ψ_{gk} :

$$\begin{aligned} \pi(\psi_{gk}|\widetilde{\mathbf{W}}, \tau^2, \Sigma_{\widetilde{\mathbf{W}}}, y_{ik}) &\propto \prod_{i=1}^n \prod_{k=1}^{k_n} f(y_{ik}|\psi_{gk}, \widetilde{\mathbf{W}}, \tau^2) \times p(\psi_{gk}) \\ &\propto \exp\left(-\frac{1}{2\tau^2} \sum_{i=1}^n \sum_{k=1}^{k_n} (y_{ik} - x_{ig}\psi_{gk} - \widetilde{w}_{ik})^2\right) \times \exp\left(-\frac{1}{20}\psi_{gk}^2\right), \end{aligned} \tag{16}$$

$$\therefore \psi_{gk}|\widetilde{\mathbf{W}}, \tau^2, \Sigma_{\widetilde{\mathbf{W}}}, y_{ik} \sim \mathcal{N}\left(\frac{M}{V}, \frac{1}{V}\right) \text{ where } M = \frac{\sum_{i=1}^n \sum_{k=1}^{k_n} (y_{ik} - \widetilde{w}_{ik})x_{ig}}{\tau^2}, V = \frac{\sum_{i=1}^n \sum_{k=1}^{k_n} x_{ig}^2}{\tau^2} + \frac{1}{10}.$$

- The conditional distribution of $\widetilde{\mathbf{W}}$:

$$\begin{aligned}\pi(\widetilde{\mathbf{W}}|\psi_{gk}, \tau^2, \Sigma_{\widetilde{\mathbf{W}}}, y_{ik}) &\propto \prod_{i=1}^n \prod_{k=1}^{k_n} f(y_{ik}|\psi_{gk}, \widetilde{\mathbf{W}}, \tau^2) \times f(\widetilde{\mathbf{W}}|\Sigma_{\widetilde{\mathbf{W}}}) \\ &\propto \exp\left(-\frac{1}{2\tau^2} \sum_{i=1}^n \sum_{k=1}^{k_n} (y_{ik} - x_{ig}\psi_{gk} - \widetilde{w}_{ik})^2\right) \times \exp\left(-\frac{1}{2\sigma^2} (\widetilde{\mathbf{W}}'\Gamma(\rho)^{-1}\widetilde{\mathbf{W}})\right),\end{aligned}\tag{17}$$

$$\therefore \widetilde{\mathbf{W}}|\psi_{gk}, \tau^2, \Sigma_{\widetilde{\mathbf{W}}}, y_{ik} \sim \mathcal{N}\left(\frac{M}{V}, \frac{1}{V}\right) \text{ where } M = \frac{\sum_{i=1}^n \sum_{k=1}^{k_n} (x_{ig}\psi_{gk} - y_{ik})}{\tau^2}, V = \frac{nk_n}{\tau^2} + \frac{\Gamma(\rho)^{-1}}{\sigma^2}.$$

- The conditional distribution of τ^2 :

$$\begin{aligned}\pi(\tau^2|\psi_{gk}, \widetilde{\mathbf{W}}, \Sigma_{\widetilde{\mathbf{W}}}, y_{ik}) &\propto \prod_{i=1}^n \prod_{k=1}^{k_n} f(y_{ik}|\psi_{gk}, \widetilde{\mathbf{W}}, \tau^2) \times p(\tau^2) \\ &\propto (\tau^2)^{-\frac{nk_n}{2}} \exp\left(-\frac{1}{2\tau^2} \sum_{i=1}^n \sum_{k=1}^{k_n} (y_{ik} - x_{ig}\psi_{gk} - \widetilde{w}_{ik})^2\right) \times (\tau^2)^{-3} \exp\left(-\frac{0.1}{\tau^2}\right) \\ &= (\tau^2)^{-\left(\frac{nk_n}{2}+2\right)-1} \exp\left(-\frac{1}{\tau^2} \left(\frac{\sum_{i=1}^n \sum_{k=1}^{k_n} (y_{ik} - x_{ig}\psi_{gk} - \widetilde{w}_{ik})^2}{2} + 0.1\right)\right),\end{aligned}\tag{18}$$

$$\therefore \tau^2|\psi_{gk}, \widetilde{\mathbf{W}}, \Sigma_{\widetilde{\mathbf{W}}}, y_{ik} \sim \text{IG}\left(\frac{nk_n}{2} + 2, \frac{\sum_{i=1}^n \sum_{k=1}^{k_n} (y_{ik} - x_{ig}\psi_{gk} - \widetilde{w}_{ik})^2}{2} + 0.1\right).$$

- The conditional distribution of $\Sigma_{\widetilde{\mathbf{W}}}$:

$$\begin{aligned}\pi(\Sigma_{\widetilde{\mathbf{W}}}| \psi_{gk}, \widetilde{\mathbf{W}}, \tau^2, y_{ik}) &\propto f(\widetilde{\mathbf{W}}|\Sigma_{\widetilde{\mathbf{W}}}) \times f(\Sigma_{\widetilde{\mathbf{W}}}|\sigma^2, \rho) \times p(\sigma^2) \times p(\rho) \\ &\propto (\sigma^2)^{-\frac{kn}{2}} \exp\left(-\frac{1}{2\sigma^2} (\widetilde{\mathbf{W}}'\Gamma(\rho)^{-1}\widetilde{\mathbf{W}})\right) \times (\sigma^2)^n \exp\left(-\sum_{i=1}^n \sum_{j=1}^n \frac{d_{ij}}{\rho}\right) \\ &\times (\sigma^2)^{-3} \exp\left(-\frac{0.1}{\sigma^2}\right) \times 1_{[0,1]}(\rho) \\ &= (\sigma^2)^{n-\frac{kn}{2}-2} \exp\left(-\left(\frac{1}{2\sigma^2} (\widetilde{\mathbf{W}}'\Gamma(\rho)^{-1}\widetilde{\mathbf{W}}) + \sum_{i=1}^n \sum_{j=1}^n \frac{d_{ij}}{\rho} + \frac{0.1}{\sigma^2}\right)\right) \times 1_{[0,1]}(\rho),\end{aligned}\tag{19}$$

where d_{ij} is distance between location i and location j .

Similarly, for discrete spatial domains, we can define the normal likelihood function $f(y_{ik}|\psi_{gk}, \widetilde{\mathbf{W}}, \tau^2, \Sigma_{\widetilde{\mathbf{W}}})$ and priors $p(\psi_{gk}), p(\tau^2)p(\Sigma_{\widetilde{\mathbf{W}}})$. Then, the joint posterior distribution for SFoFR (basis space) as $\pi(\psi_{gk}, \widetilde{\mathbf{W}}, \tau^2, \Sigma_{\widetilde{\mathbf{W}}}|y_{ik}) \propto \prod_{i=1}^n \prod_{k=1}^{k_n} f(y_{ik}|\psi_{gk}, \widetilde{\mathbf{W}}, \tau^2) f(\widetilde{\mathbf{W}}|\nu) p(\psi_{gk}) p(\tau^2) p(\Sigma_{\widetilde{\mathbf{W}}})$. Here, we use independent normal conjugate priors for $\psi_{gk} \sim \mathcal{N}(0, 10)$, an inverse gamma conjugate prior for $\tau^2 \sim \mathcal{IG}(2, 0.1)$ and a Gamma conjugate prior for $\nu \sim \mathcal{G}(0.5, \frac{1}{2,000})$. Let $\mathbf{Q} = \text{diag}(\mathbf{D}\mathbf{1}) - \mathbf{D}$ be a precision matrix, and $\Sigma_{\widetilde{\mathbf{W}}} = \nu\mathbf{Q}$. Then, the full conditional distributions are derived as

- The conditional distribution of ψ_{gk} :

$$\begin{aligned} \pi(\psi_{gk}|\widetilde{\mathbf{W}}, \tau^2, \Sigma_{\widetilde{\mathbf{W}}}, y_{ik}) &\propto \prod_{i=1}^n \prod_{k=1}^{k_n} f(y_{ik}|\psi_{gk}, \widetilde{\mathbf{W}}, \tau^2) \times p(\psi_{gk}) \\ &\propto \exp\left(-\frac{1}{2\tau^2}(y_{ik} - x_{ig}\psi_{gk} - \widetilde{w}_{ik})^2\right) \times \exp\left(-\frac{1}{20}\psi_{gk}^2\right), \end{aligned} \quad (20)$$

$$\therefore \psi_{gk}|\widetilde{\mathbf{W}}, \tau^2, \Sigma_{\widetilde{\mathbf{W}}}, y_{ik} \sim \mathcal{N}\left(\frac{M}{V}, \frac{1}{V}\right) \text{ where } M = \frac{\sum_{i=1}^n \sum_{k=1}^{k_n} (y_{ik} - \widetilde{w}_{ik})x_{ig}}{\tau^2}, V = \frac{\sum_{i=1}^n \sum_{k=1}^{k_n} x_{ig}^2}{\tau^2} + \frac{1}{10}.$$

- The conditional distribution of $\widetilde{\mathbf{W}}$:

$$\begin{aligned} \pi(\widetilde{\mathbf{W}}|\psi_{gk}, \tau^2, \Sigma_{\widetilde{\mathbf{W}}}, y_{ik}) &\propto \prod_{i=1}^n \prod_{k=1}^{k_n} f(y_{ik}|\psi_{gk}, \widetilde{\mathbf{W}}, \tau^2) \times f(\widetilde{\mathbf{W}}|\nu) \\ &\propto \exp\left(-\frac{1}{2\tau^2} \sum_{i=1}^n \sum_{k=1}^{k_n} (y_{ik} - x_{ig}\psi_{gk} - \widetilde{w}_{ik})^2\right) \times \exp\left(\frac{\nu}{2}(\widetilde{\mathbf{W}}'\mathbf{Q}\widetilde{\mathbf{W}})\right), \end{aligned} \quad (21)$$

$$\therefore \widetilde{\mathbf{W}}|\psi_{gk}, \tau^2, \Sigma_{\widetilde{\mathbf{W}}}, y_{ik} \sim \mathcal{N}\left(\frac{M}{V}, \frac{1}{V}\right) \text{ where } M = \frac{\sum_{i=1}^n \sum_{k=1}^{k_n} (x_{ig}\psi_{gk} - y_{ik})}{\tau^2}, V = \frac{nk_n}{\tau^2} - \nu\mathbf{Q}.$$

- The conditional distribution of τ^2 :

$$\begin{aligned} \pi(\tau^2|\psi_{gk}, \widetilde{\mathbf{W}}, \Sigma_{\widetilde{\mathbf{W}}}, y_{ik}) &\propto \prod_{i=1}^n \prod_{k=1}^{k_n} f(y_{ik}|\psi_{gk}, \widetilde{\mathbf{W}}, \tau^2) \times p(\tau^2) \\ &\propto (\tau^2)^{-\frac{nk_n}{2}} \exp\left(-\frac{1}{2\tau^2} \sum_{i=1}^n \sum_{k=1}^{k_n} (y_{ik} - x_{ig}\psi_{gk} - \widetilde{w}_{ik})^2\right) \times (\tau^2)^{-3} \exp\left(-\frac{0.1}{\tau^2}\right) \\ &= (\tau^2)^{-\left(\frac{nk_n}{2}+2\right)-1} \exp\left(-\frac{1}{\tau^2} \left(\frac{\sum_{i=1}^n \sum_{k=1}^{k_n} (y_{ik} - x_{ig}\psi_{gk} - \widetilde{w}_{ik})^2}{2} + 0.1\right)\right), \end{aligned} \quad (22)$$

$$\therefore \tau^2 | \psi_{gk}, \widetilde{\mathbf{W}}, \Sigma_{\widetilde{\mathbf{W}}}, y_{ik} \sim \mathcal{IG} \left(\frac{nk_n}{2} + 2, \frac{\sum_{i=1}^n \sum_{k=1}^{k_n} (y_{ik} - x_{ig} \psi_{gk} - \widetilde{w}_{ik})^2}{2} + 0.1 \right).$$

- The conditional distribution of $\Sigma_{\widetilde{\mathbf{W}}}$:

$$\begin{aligned} \pi(\Sigma_{\widetilde{\mathbf{W}}} | \psi_{gk}, \widetilde{\mathbf{W}}, \tau^2, y_{ik}) &\propto f(\widetilde{\mathbf{W}} | \Sigma_{\widetilde{\mathbf{W}}}) \times p(\Sigma_{\widetilde{\mathbf{W}}}) \\ &\propto (\nu)^{-\frac{n}{2}} \exp \left(\frac{\nu}{2} (\widetilde{\mathbf{W}}' \mathbf{Q} \widetilde{\mathbf{W}}) \right) \times (\nu)^{\frac{n}{2}} \exp \left(-\frac{n}{2,000} \nu \right) \\ &= (\nu)^{1-1} \exp \left(- \left(\frac{\widetilde{\mathbf{W}}' \mathbf{Q} \widetilde{\mathbf{W}}}{2} + \frac{n}{2,000} \right) \nu \right), \end{aligned} \quad (23)$$

$$\therefore \Sigma_{\widetilde{\mathbf{W}}} | \psi_{gk}, \widetilde{\mathbf{W}}, \tau^2, y_{ik} \sim \mathcal{G} \left(1, \frac{\widetilde{\mathbf{W}}' \mathbf{Q} \widetilde{\mathbf{W}}}{2} + \frac{n}{2,000} \right).$$

A.2 Full Conditionals for PSFoFR

Let $f(y_{ik} | \psi_{gk}, \boldsymbol{\delta}, \tau^2, \Sigma_{\boldsymbol{\delta}})$ be the normal likelihood function with priors $p(\psi_{gk}), p(\tau^2), p(\Sigma_{\boldsymbol{\delta}})$ where $\Sigma_{\boldsymbol{\delta}} = \sigma^2 \mathbf{P}' \mathbf{Q} \mathbf{P}$ is covariance structure of $\boldsymbol{\delta}$. Then we can define the joint posterior distribution for PSFoFR (basis space) as $\pi(\psi_{gk}, \boldsymbol{\delta}, \tau^2, \Sigma_{\boldsymbol{\delta}} | y_{ik}) \propto \prod_{i=1}^n \prod_{k=1}^{k_n} f(y_{ik} | \psi_{gk}, \mathbf{P}, \boldsymbol{\delta}, \tau^2) f(\boldsymbol{\delta} | \Sigma_{\boldsymbol{\delta}}) p(\psi_{gk}) p(\tau^2) p(\Sigma_{\boldsymbol{\delta}})$. Here, we use independent normal conjugate priors for $\psi_{gk} \sim \mathcal{N}(0, 10)$, an inverse gamma conjugate priors for $\tau^2 \sim \mathcal{IG}(2, 0.1)$ and $\sigma^2 \sim \mathcal{G}(0.5, \frac{1}{2,000})$. We define $(\mathbf{P}\boldsymbol{\delta})_{ik}$ as an element of $\mathbf{P}\boldsymbol{\delta}$ at i -th row and k -th column. From this, we can obtain the full conditionals of PSFoFR as follows:

- The conditional distribution of ψ_{gk} :

$$\begin{aligned} \pi(\psi_{gk} | \boldsymbol{\delta}, \tau^2, \Sigma_{\boldsymbol{\delta}}, y_{ik}) &\propto \prod_{i=1}^n \prod_{k=1}^{k_n} f(y_{ik} | \psi_{gk}, \mathbf{P}, \boldsymbol{\delta}, \tau^2) \times p(\psi_{gk}) \\ &\propto \exp \left(-\frac{1}{2\tau^2} \sum_{i=1}^n \sum_{k=1}^{k_n} (y_{ik} - x_{ig} \psi_{gk} - (\mathbf{P}\boldsymbol{\delta})_{ik})^2 \right) \times \exp \left(-\frac{1}{20} \psi_{gk}^2 \right), \end{aligned} \quad (24)$$

$$\therefore \psi_{gk} | \boldsymbol{\delta}, \tau^2, \Sigma_{\boldsymbol{\delta}}, y_{ik} \sim \mathcal{N} \left(\frac{M}{V}, \frac{1}{V} \right) \text{ where } M = \frac{\sum_{i=1}^n \sum_{k=1}^{k_n} (y_{ik} - \widetilde{w}_{ik}) x_{ig}}{\tau^2}, V = \frac{\sum_{i=1}^n \sum_{k=1}^{k_n} x_{ig}^2}{\tau^2} + \frac{1}{10}.$$

- The conditional distribution of τ^2 :

$$\begin{aligned}
\pi(\tau^2|\psi_{gk}, \boldsymbol{\delta}, \boldsymbol{\Sigma}_{\boldsymbol{\delta}}, y_{ik}) &\propto \prod_{i=1}^n \prod_{k=1}^{k_n} f(y_{ik}|\psi_{gk}, \mathbf{P}, \boldsymbol{\delta}, \tau^2) \times p(\tau^2) \\
&\propto (\tau^2)^{-\frac{nk_n}{2}} \exp\left(-\frac{1}{2\tau^2} \sum_{i=1}^n \sum_{k=1}^{k_n} (y_{ik} - x_{ig}\psi_{gk} - (\mathbf{P}\boldsymbol{\delta})_{ik})^2\right) \times (\tau^2)^{-3} \exp\left(-\frac{0.1}{\tau^2}\right) \\
&= (\tau^2)^{-\left(\frac{nk_n}{2}+2\right)-1} \exp\left(-\frac{1}{\tau^2} \left(\frac{\sum_{i=1}^n \sum_{k=1}^{k_n} (y_{ik} - x_{ig}\psi_{gk} - (\mathbf{P}\boldsymbol{\delta})_{ik})^2}{2} + 0.1\right)\right),
\end{aligned} \tag{25}$$

$$\therefore \tau^2|\psi_{gk}, \boldsymbol{\delta}, \boldsymbol{\Sigma}_{\boldsymbol{\delta}}, y_{ik} \sim \text{IG}\left(\frac{nk_n}{2} + 2, \frac{\sum_{i=1}^n \sum_{k=1}^{k_n} (y_{ik} - x_{ig}\psi_{gk} - (\mathbf{P}\boldsymbol{\delta})_{ik})^2}{2} + 0.1\right).$$

- The conditional distribution of $\boldsymbol{\delta}$:

$$\begin{aligned}
\pi(\boldsymbol{\delta}|\psi_{gk}, \tau^2, \boldsymbol{\Sigma}_{\boldsymbol{\delta}}, y_{ik}) &\propto \prod_{i=1}^n \prod_{k=1}^{k_n} f(y_{ik}|\psi_{gk}, \mathbf{P}, \boldsymbol{\delta}, \tau^2) \times f(\boldsymbol{\delta}|\boldsymbol{\Sigma}_{\boldsymbol{\delta}}) \\
&\propto \exp\left(-\frac{1}{2\tau^2} \sum_{i=1}^n \sum_{k=1}^{k_n} (y_{ik} - x_{ig}\psi_{gk} - (\mathbf{P}\boldsymbol{\delta})_{ik})^2\right) \times \exp\left(-\frac{\sigma^2}{2} \boldsymbol{\delta}'\mathbf{P}'\mathbf{Q}\mathbf{P}\boldsymbol{\delta}\right),
\end{aligned} \tag{26}$$

$$\therefore \boldsymbol{\delta}|\psi_{gk}, \tau^2, \boldsymbol{\Sigma}_{\boldsymbol{\delta}}, y_{ik} \sim \mathcal{N}\left(\frac{M}{V}, \frac{1}{V}\right) \text{ where } M = \frac{\sum_{i=1}^n \sum_{k=1}^{k_n} (x_{ig}\psi_{gk} - y_{ik})\mathbf{P}}{\tau^2}, V = \frac{nk_n\mathbf{P}'\mathbf{P}}{\tau^2} + \sigma^2\mathbf{P}'\mathbf{Q}\mathbf{P}.$$

- The conditional distribution of $\boldsymbol{\Sigma}_{\boldsymbol{\delta}}$:

$$\begin{aligned}
\pi(\boldsymbol{\Sigma}_{\boldsymbol{\delta}}|\psi_{gk}, \boldsymbol{\delta}, \tau^2, y_{ik}) &\propto f(\boldsymbol{\delta}|\boldsymbol{\Sigma}_{\boldsymbol{\delta}}) \times p(\boldsymbol{\Sigma}_{\boldsymbol{\delta}}) \\
&\propto (\sigma^2)^{\frac{p}{2}} \exp\left(-\frac{\sigma^2}{2} \boldsymbol{\delta}'\mathbf{P}'\mathbf{Q}\mathbf{P}\boldsymbol{\delta}\right) \times (\sigma^2)^{-\frac{p}{2}} \exp\left(-\frac{p}{2,000}\sigma^2\right) \\
&= (\sigma^2)^{1-1} \exp\left(-\left(\frac{\boldsymbol{\delta}'\mathbf{P}'\mathbf{Q}\mathbf{P}\boldsymbol{\delta}}{2} + \frac{p}{2,000}\right)\sigma^2\right), \\
\therefore \boldsymbol{\Sigma}_{\boldsymbol{\delta}}|\psi_{gk}, \boldsymbol{\delta}, \tau^2, y_{ik} &\sim \mathcal{G}\left(1, \frac{\boldsymbol{\delta}'\mathbf{P}'\mathbf{Q}\mathbf{P}\boldsymbol{\delta}}{2} + \frac{p}{2,000}\right).
\end{aligned} \tag{27}$$

B Estimated Regression Functions for SFoFR in the Simulation

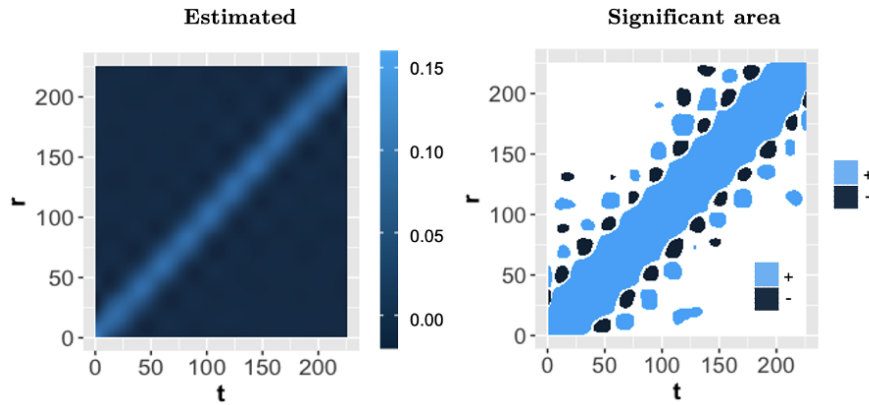


Figure 9: The estimated regression functions from SFoFR. Significant areas in the functions are detected from $\alpha = 0.05$. Sky blue colors represent positive significant areas, whereas dark blue colors represent negative significant areas.

C Simulation Results with Different Basis Functions

C.1 Fourier Basis

We use $n = 700$ samples for training and $n_{cv} = 300$ samples for prediction. For PSFoFR, we run the MCMC algorithm for 70,000 iterations with 50,000 discarded for burn-in, and 1,000 thinned samples are obtained from the remaining 20,000. We use $k_n = 19$ and $g_n = 13$; the number of basis functions is chosen by minimizing GCV error. We set the rank values as 5% of the sample size.

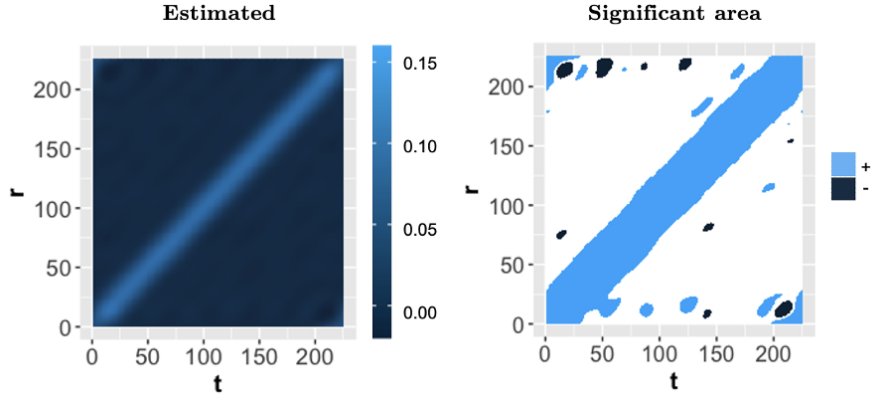


Figure 10: The estimated regression functions from PSFoFR with Fourier basis. Significant areas in the functions are detected from $\alpha = 0.05$. Sky blue colors represent positive significant areas, whereas dark blue colors represent negative significant areas.

C.2 FPC Basis

We use $n = 700$ samples for training and $n_{cv} = 300$ samples for prediction. For PSFoFR, we run the MCMC algorithm for 70,000 iterations with 50,000 discarded for burn-in, and 1,000 thinned samples are obtained from the remaining 20,000. We use $k_n = 11$ and $g_n = 171$. We set k_n and g_n to achieve the function of variance explained at 90%. As in the other basis functions, we set the rank values as 5% of the sample size.

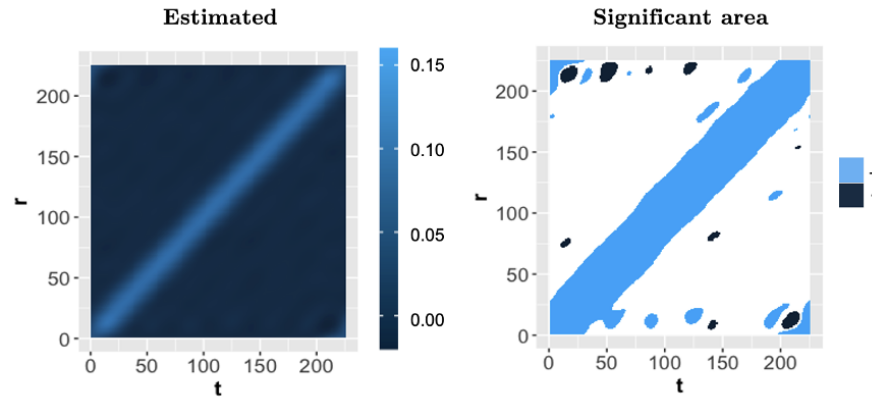


Figure 11: The estimated regression function from PSFoFR with FPC basis. Significant areas in the functions are detected from $\alpha = 0.05$. Sky blue colors represent positive significant areas, whereas dark blue colors represent negative significant areas.

C.3 Comparison

Basis Type	MSPE	MSE	Time
Fourier	0.124	0.004	45
FPC	0.125	0.004	27

Table 2: Inference results for the simulated datasets. MSPE, MSE, and computing time (min) are reported.

Figures 10, 11 indicate that the estimated regression functions are quantitatively similar to those from the B-spline basis expansion in the main manuscript. Although the overall trend is similar, we observe that the estimated functions from FPC are rough compared to the other two basis functions. Table 2 shows that the results using Fourier and FPC bases are similar. However, the MSPE is higher compared to the B-spline basis.

D Mean Functions of Functional Variables in Real Data Examples

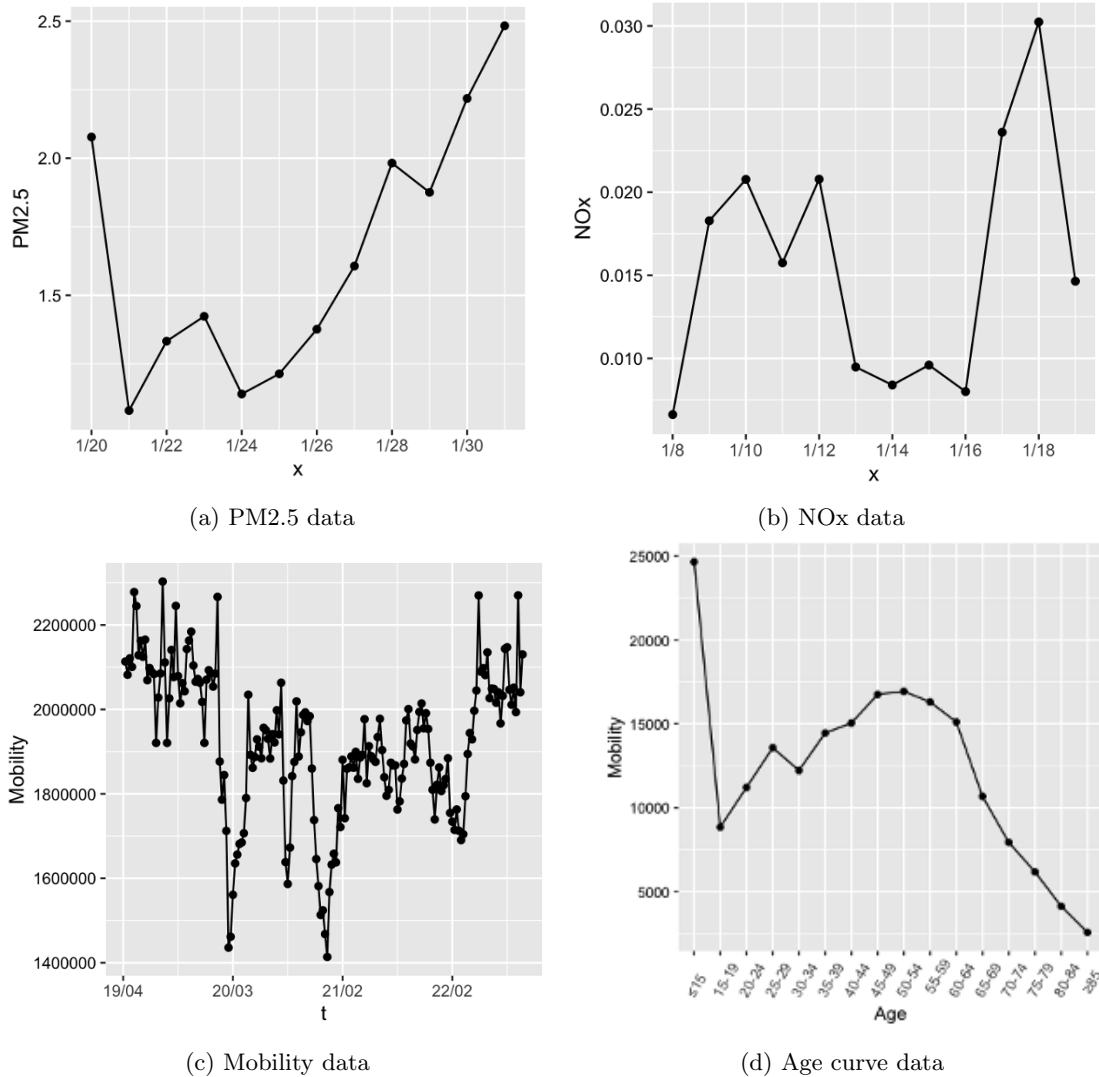


Figure 12: Mean functions of functional variables in real data examples.

References

Aristizabal, J.-P., Giraldo, R., and Mateu, J. (2019). Analysis of variance for spatially correlated functional data: Application to brain data. *Spatial Statistics*, 32:100381.

- Banerjee, S., Gelfand, A. E., Finley, A. O., and Sang, H. (2008). Gaussian predictive process models for large spatial data sets. *Journal of the Royal Statistical Society. Series B (Statistical Methodology)*, 70(4):825–848.
- Besag, J. and Kooperberg, C. (1995). On conditional and intrinsic autoregressions. *Biometrika*, 82(4):733–746.
- Caballero, W., Giraldo, R., and Mateu, J. (2013). A universal kriging approach for spatial functional data. *Stochastic Environmental Research and Risk Assessment*, 27(7):1553–1563.
- Cardot, H., Ferraty, F., and Sarda, P. (1999). Functional linear model. *Statistics & Probability Letters*, 45(1):11–22.
- de Valpine, P., Turek, D., Paciorek, C. J., Anderson-Bergman, C., Lang, D. T., and Bodik, R. (2017). Programming with models: Writing statistical algorithms for general model structures with NIMBLE. *Journal of Computational and Graphical Statistics*, 26(2):403–413.
- Delicado, P., Giraldo, R., Comas, C., and Mateu, J. (2010). Statistics for spatial functional data: some recent contributions. *Environmetrics: The official journal of the International Environmetrics Society*, 21(3-4):224–239.
- Flegal, J. M., Haran, M., and Jones, G. L. (2008). Markov Chain Monte Carlo: Can we trust the third significant figure? *Statistical Science*, 23(2):250–260.
- Fu, S., Liu, P., He, X., Song, Y., Liu, J., Zhang, C., and Mu, Y. (2023). Significantly mitigating pm_{2.5} pollution level via reduction of nox emission during wintertime. *Science of the Total Environment*, 898:165350.
- Giraldo, R., Delicado, P., and Mateu, J. (2011). Ordinary kriging for function-valued spatial data. *Environmental and Ecological Statistics*, 18(3):411–426.
- Goulard, M. and Voltz, M. (1993). *Geostatistical Interpolation of Curves: A Case Study in Soil Science*, pages 805–816. Springer.
- Griffith, D. A. (2004). A spatial filtering specification for the autologistic model. *Environment and Planning A*, 36(10):1791–1811.

- Grujic, O. and Menafoglio, A. (2017). *fdagstat, an R package*. R package version 1.0.
- Ha, J., Lee, J., Choi, S., and Park, S. (2023). Covid-19 waves and their characteristics in the seoul metropolitan area (jan 20, 2020–aug 31, 2022). *Public Health Weekly Report*, 16(5):111–136.
- Huang, P.-C., Hung, H.-M., Lai, H.-C., and Chou, C. C.-K. (2024). Assessing the effectiveness of so₂, nox, and nh₃ emission reductions in mitigating winter pm 2.5 in taiwan using cmaq model. *EGUsphere*, 2024:1–30.
- Hughes, J. and Haran, M. (2013). Dimension reduction and alleviation of confounding for spatial generalized linear mixed models. *Journal of the Royal Statistical Society. Series B (Statistical Methodology)*, 75(1):139–159.
- Ivanescu, A. E., Staicu, A.-M., Scheipl, F., and Greven, S. (2015). Penalized function-on-function regression. *Computational Statistics*, 30:539–568.
- Jones, G. L., Haran, M., Caffo, B. S., and Neath, R. (2006). Fixed-width output analysis for Markov Chain Monte Carlo. *Journal of the American Statistical Association*, 101(476):1537–1547.
- Kang, H. B., Jung, Y. J., and Park, J. (2023). Fast Bayesian functional regression for non-Gaussian spatial data. *Bayesian Analysis*, 1(1):1–32.
- Kang, Y. H. and Kim, S. (2022). Seasonal PM management: (i) What emissions should be reduced? *Journal of Korean Society for Atmospheric Environment*, 38(5):746–763.
- Katzfuss, M. (2017). A multi-resolution approximation for massive spatial datasets. *Journal of the American Statistical Association*, 112(517):201–214.
- Kim, J. S., Staicu, A.-M., Maity, A., Carroll, R. J., and Ruppert, D. (2018). Additive function-on-function regression. *Journal of Computational and Graphical Statistics*, 27(1):234–244.
- Kowal, D. R. and Bourgeois, D. C. (2020). Bayesian function-on-scalars regression for high dimensional data. *Journal of Computational and Graphical Statistics*, 29(3):629–638.
- Lee, B. S. and Haran, M. (2022). PICAR: An efficient extendable approach for fitting hierarchical spatial models. *Technometrics*, 64(2):187–198.

- Lee, B. S. and Park, J. (2023). A scalable partitioned approach to model massive nonstationary non-Gaussian spatial datasets. *Technometrics*, 65(1):105–116.
- Leibensperger, E., Mickley, L., Jacob, D., and Barrett, S. (2011). Intercontinental influence of NO_x and CO emissions on particulate matter air quality. *Atmospheric Environmen*, 45(19):3318–3324.
- Lindgren, F. and Rue, H. (2015). Bayesian spatial modelling with R-INLA. *Journal of statistical software*, 63(19).
- Martínez-Hernández, I. and Genton, M. G. (2020). Recent developments in complex and spatially correlated functional data. *Brazilian Journal of Probability and Statistics*, 34(2):204–229.
- Menafoglio, A., Secchi, P., and Dalla Rosa, M. (2013). A universal kriging predictor for spatially dependent functional data of a Hilbert space. *Electronic Journal of Statistics*, 7:2209–2240.
- Meyer, M. J., Coull, B. A., Versace, F., Cinciripini, P., and Morris, J. S. (2015). Bayesian function-on-function regression for multilevel functional data. *Biometrics*, 71(3):563–574.
- Ministry of the Environment Government of Japan, I. (2023). Japan PM 2.5 data. <https://soramame.env.go.jp/> [Accessed: (2023.6.30)].
- Moran, P. A. (1950). Notes on continuous stochastic phenomena. *Biometrika*, 37(1/2):17–23.
- Morris, J. S. and Carroll, R. J. (2006). Wavelet-based functional mixed models. *Journal of the Royal Statistical Society. Series B (Statistical Methodology)*, 68(2):179–199.
- Müller, H.-G. and Stadtmüller, U. (2005). Generalized functional linear models. *The Annals of Statistics*, 33(2):774–805.
- Park, J. and Lee, S. (2022). A projection-based Laplace approximation for spatial latent variable models. *Environmetrics*, 33(1):e2703.
- Park, Y., Li, B., and Li, Y. (2023). Crop yield prediction using Bayesian spatially varying coefficient models with functional predictors. *Journal of the American Statistical Association*, 118(541):70–83.

- Pineda-Ríos, W., Giraldo, R., and Porcu, E. (2019). Functional SAR models: With application to spatial econometrics. *Spatial Statistics*, 29:145–159.
- Ramsay, J. O. and Silverman, B. W. (2005). *Functional data analysis*. Springer.
- Reiss, P. T., Goldsmith, J., Shang, H. L., and Ogden, R. T. (2017). Methods for scalar-on-function regression. *International Statistical Review*, 85(2):228–249.
- Reiss, P. T., Huang, L., and Mennes, M. (2010). Fast function-on-scalar regression with penalized basis expansions. *The international journal of biostatistics*, 6(1).
- Římalová, V., Fišerová, E., Menafoglio, A., and Pini, A. (2022). Inference for spatial regression models with functional response using a permutational approach. *Journal of Multivariate Analysis*, 189:104893.
- Scheipl, F., Gertheiss, J., and Greven, S. (2016). Generalized functional additive mixed models. *Electronic Journal of Statistics*, 10(1):1455–1492.
- Stein, M. L. (2012). *Interpolation of spatial data some theory for kriging*. Springer Science & Business Media.
- Zhang, L., Baladandayuthapani, V., Zhu, H., Baggerly, K. A., Majewski, T., Czerniak, B. A., and Morris, J. S. (2016). Functional CAR models for large spatially correlated functional datasets. *Journal of the American Statistical Association*, 111(514):772–786.